NASA TECHNICAL NOTE

NASA TN D-2807

EVALUATION OF PILOT'S ABILITY TO STABILIZE A FLEXIBLE LAUNCH VEHICLE DURING FIRST-STAGE BOOST

by Gordon H. Hardy and James V. West

Ames Research Center

and

Robert W. Gunderson

George C. Marshall Space Flight Center

NATIONAL AERONAUTICS AND SPACE ADMINISTRATION • WASHINGTON, D. C. • MAY 1965

NASA TN D-2807

EVALUATION OF PILOT'S ABILITY TO STABILIZE A FLEXIBLE LAUNCH VEHICLE DURING FIRST-STAGE BOOST

By Gordon H. Hardy and James V. West

Ames Research Center
Moffett Field, Calif.

and

Robert W. Gunderson

George C. Marshall Space Flight Center
Huntsville, Ala.

NATIONAL AERONAUTICS AND SPACE ADMINISTRATION

For sale by the Clearinghouse for Federal Scientific and Technical Information
Springfield, Virginia 22151 – Price $3.00

EVALUATION OF PILOT'S ABILITY TO STABILIZE A FLEXIBLE LAUNCH VEHICLE DURING FIRST-STAGE BOOST

By Gordon H. Hardy and James V. West
Ames Research Center

and

Robert W. Gunderson
Marshall Space Flight Center

SUMMARY

The feasibility of manned participation in the control of the atmospheric flight of a large launch vehicle was investigated. Studies included simulation of rigid, elastic, and fuel-sloshing dynamics of the Saturn V lunar mission vehicle. Fixed cockpit and centrifuge results indicate that pilots could satisfactorily stabilize the vehicle and reduce structural loads. They were also able to handle wide variations in vehicle parameters and to handle certain failure situations.

INTRODUCTION

There has been considerable speculation that pilot participation in the guidance and control of the Saturn V launch vehicle could increase the probability of over-all mission success. Some study of piloted control of large launch vehicles has already been completed, most notably for the Titan III (refs. 1-3), and the somewhat earlier investigation by Holleman and Armstrong (ref. 4). These investigations have shown that the problem of controlling launch vehicles manually may be broken into two separate phases. The first is the atmospheric flight phase for which the guidance system requirements are relatively insignificant. The primary problems here are attitude stabilization and aerodynamic load reduction of a large, flexible, and usually aerodynamically unstable vehicle. These problems are further complicated by wind disturbances and in some instances by propellant-sloshing dynamics. During the second phase of flight, outside the sensible atmosphere, the problem areas reverse. Since the vehicle is usually much stiffer (second and third stages of flight) and there are no atmospheric disturbances, the attitude stabilization task is relieved. During this second phase of flight, though, the vehicle must be guided precisely into some type of orbit. The orbit injection requirement makes guidance the primary problem during the second or guidance phase of flight. The previous investigations mentioned have demonstrated the feasibility of manually controlling both phases of flight for particular vehicles and particular mission profiles.

While much can be learned from these studies, the large differences of the Saturn V vehicle and mission objectives make it difficult to extrapolate

the results. Consequently the Marshall Space Flight Center (MSFC) and Ames Research Center (ARC) are currently engaged in a joint feasibility study to determine the possibility of manually controlling the Saturn V launch vehicle during both phases of flight, from lift-off through lunar orbit injection. Earth-orbital phases are not being considered.

The purpose of this report is to present the results obtained for the atmospheric flight phase. The high fineness ratio, area distribution, and large mass to area ratio of the Saturn V configuration distinguish it from previously investigated vehicles. Because of the large mass to area ratio and the unwinged payload (Apollo capsule), the level of aerodynamic instability is relatively low. The high fineness ratio manifests itself in large elastic motions of the vehicle. Since the frequencies of these elastic motions are relatively low (nearing pilot control frequencies), it was felt they could present several problems. Among these are the requirements placed on the stability augmentation system and the motion cues felt by the pilot (located near the forward end). Previous studies had investigated the effects of thrust and rigid body accelerations on the pilot's control capabilities; the present study included an investigation of the elastic motion accelerations.

The simulation used both a fixed-base cockpit and the Ames five-degrees-of-freedom centrifuge. The mathematical simulation was carried out on an electronic analog computer and included five rigid body degrees of motion, two modes of elastic body motions, and fuel-sloshing dynamics. Guidance consisted of a pitch attitude open-loop time program. In addition to stabilizing attitude and reducing structural loads due to the wind, the pilot was required to roll the vehicle to the proper downrange heading immediately after take-off.

NOTATION

a_1	gain coefficient in rate loop, sec
c.g.	center of gravity
$F_\alpha, F_\varphi, F_\beta, M_\alpha, M_\beta, M_\beta', K_{1i}, K_{2i}, K_{3i}, K_{4i}, K_{5i}$	time varying coefficients
g	sea-level value of earth's acceleration, m/sec^2
g_2	gain coefficient in accelerometer loop, $deg/m/sec^2$
I	vehicle moment of inertia, $kg\text{-}m\text{-}sec^2$
l_a	distance from vehicle c.g. to accelerometer measured positive forward, meters
m	mass of the vehicle, $kg\text{-}sec^2/m$
m_{s_i}	mass of the ith fuel-sloshing mass, $kg\text{-}sec^2/m$

$\frac{M}{M_D}$	rigid body bending moment at specified station divided by design value
q	dynamic presssure, kg/m^2
s	Laplace operator, 1/sec
V	nominal vehicle velocity, m/sec
x_i	vehicle c.g. location with respect to nominal location, meters
x_{si}	distance to the ith fuel-sloshing mass measured positive aft, meters
α_i	aerodynamic angle of attack, deg
α_{w_i}	component of angle of attack due to wind, deg
β_i	engine gimbal angle, deg
$\ddot{\gamma}_i$	accelerometer output, m/sec^2
$\ddot{\gamma}_i^*$	rigid body component of accelerometer output, m/sec^2
ζ	damping ratio
ζ_{b_i}	damping ratio of ith bending mode
ζ_{s_i}	damping ratio of ith fuel tank
η_{ji}	ith generalized elastic bending mode amplitude in j direction
ξ_{ji}	amplitude of motion of ith fuel-tank sloshing mass in j direction, meters
φ_i	total attitude angle with respect to a space fixed coordinate system, deg
$\Delta\varphi_i$	attitude error sensed by the inertial navigator, deg
$\Delta\varphi_i^*$	rigid body attitude error, deg
χ_i	nominal vehicle attitude with respect to a space fixed coordinate system, deg
ω_n	natural frequency, 1/sec
ω_{b_i}	natural frequency of ith bending mode
ω_{s_i}	natural frequency of ith fuel tank

Subscripts

C command

P pitch

Y yaw

R roll

1 component along x_1 axis

2 component along x_2 axis

3 component along x_3 axis

DESCRIPTION OF SIMULATION

Vehicle Description

The example vehicle used in this study was the Saturn V launch vehicle as defined for the Apollo lunar landing mission. As shown in figure 1, the vehicle configuration consists of three booster stages and the Apollo spacecraft. Over-all vehicle length is 360 feet and the maximum diameter is 396 inches (not including fins). Fully fueled, the vehicle weighs approximately 6,000,000 pounds. The launch vehicle consists of three liquid fueled stages. The S-IC, or first stage, is powered by five F-1 engines with a total thrust of 7,500,000 pounds.

The Saturn V launch vehicle has an inertial navigation and guidance system independent of the one contained in the Apollo spacecraft. A control system computer and necessary sensors are also located in the launch vehicle.

Trajectory Description

The present report is concerned with the trajectory from launch through first stage burnout. This stage follows a gravity turn trajectory for 150 seconds and separates at approximately 60,000 meters altitude with a velocity of 2,350 meters per second. The maximum thrust-to-weight ratio is 4.7 and the maximum dynamic pressure of 3,650 kg/m^2 occurs at an altitude of 13,000 meters.

Wind Environment

The primary trajectory disturbance during the first stage of flight is the wind environment. The wind environment used in this study is based on statistical analysis of wind measurements taken at the Air Force Eastern Test

Range (formerly Atlantic Missile Range), Cape Kennedy Launch Area. Values of steady-state wind, wind shear, gusts, and turbulence are considered. The steady-state winds were assumed horizontal with no restriction on direction.

Figure 2 presents the wind used for this report. The maximum wind speed is 75 meters per second in the sensible atmosphere (below 30,000 meters), while the maximum value of wind shear occurs near the point of maximum dynamic pressure. Because of the large mass to area ratio of Saturn V, low amplitude, high frequency gusts and turbulence have little effect on rigid body vehicle loading and control. In addition, reference 5 shows that for this class vehicle the effects of gusts and turbulence on elastic body dynamics are small. Consequently, they were not included in the present study. Quartering headwinds and tailwinds were found more difficult to control than winds all in one axis. Consequently, the wind profile of figure 2 was assumed to act 45°, 135°, 225°, and 315° relative to vehicle heading. The directions were chosen in a random sequence from run to run to help eliminate pilot learning of a particular wind.

Guidance and Control Constraints

The principal constraints placed on the launch guidance and control system are guidance accuracy and structural loads. Since the study of the present report considers only the first stage of flight, structural loads were the primary constraint.

The performance measures used in this study to show how well the system has satisfied the design constraints are described in the following paragraphs.

The primary performance measure used was the body bending moment occurring at a critical location on the vehicle. This bending moment was calculated with the expression

$$M_x = \frac{\partial M_x}{\partial \alpha}\,\alpha + \frac{\partial M_x}{\partial \beta}\,\beta + \frac{\partial M_x}{\partial \ddot{\eta}_1}\,\ddot{\eta}_1 + \frac{\partial M_x}{\partial \ddot{\eta}_2}\,\ddot{\eta}_2$$

where

M_x body bending moment at station x

$\frac{\partial M_x}{\partial \alpha}$ function of mass distribution and aerodynamic loading, constant at a given time of flight at station x

$\frac{\partial M_x}{\partial \beta}$ function of mass distribution and thrust, constant for a given time of flight at station x

$\frac{\partial M_x}{\partial \ddot{\eta}_i}$ sensitivity of M_x to the ith generalized elastic mode acceleration, constant at a given time of flight at station x

and $\alpha, \beta, \ddot{\eta}_i$ are the angle of attack, engine angle, and ith generalized elastic mode acceleration, respectively. The resultant of the pitch and yaw bending moments, normalized to unity at the limit design moment, was used for data presentation. It should be noted that fuel sloshing will contribute to the body bending moment, but that data relating sloshing mass accelerations to body bending moment were not available at the time of the study. Preliminary data indicate the contribution will be small (less than 10 percent of the design value). Sloshing mass accelerations, where calculated, are presented for reference.

The elastic mode accelerations contribute to the motion cues felt by the pilot. Since these may be objectionable, a design goal was to minimize them. Data are presented in terms of the elastic body accelerations felt by the pilot.

A measure of how well the pilot could control to the nominal trajectory was obtained by measuring the distance and velocity dispersions normal to the nominal trajectory at the first-stage cutoff point. As mentioned previously, however, trajectory control during the first stage of the boost profile is considered a less stringent constraint than structural loading.

The final performance measure used was the numerical Cooper Pilot Opinion Rating System shown in figure 3. This rating is the pilot's subjective opinion of how well he was able to control the system with respect to the task assigned. Reference 6 describes the Cooper Rating System in detail.

Control System Description

Attitude of the Saturn V during the powered flight of the first stage is controlled by swiveling the four outboard F-1 engines. The center engine does not swivel. The outboard engines are each swiveled in the pitch and yaw planes by pitch and yaw hydraulic actuators. For roll control a combination of pitch and yaw actuators is used.

The roll control system used during the study was a simple rate augmentation system while figure 4 shows the configuration of the pitch and yaw nominal manual control system studied. It will be noted that the pitch and yaw augmentation system consists of a single (rate) loop. The rate gyros were located at station 2470 on the vehicle for this study. Attitude, attitude error, attitude rate, and accelerometer signals from body-mounted normal accelerometers mounted in the second stage are displayed to the pilot. The inertial platform for sensing attitude was located at station 3260 in figure 1.

The basic configuration, or loop structure, was determined by rigid body studies. Introducing elastic body dynamics dictated the addition of two filters (rate augmentation filter and controller output filter) to maintain system stability.

The rigid body vehicle is inherently unstable because of the aft location of the c.g. with respect to the center of pressure. This instability varies

with time of flight and reaches a peak (ω_n^2 of the short period mode equal to about -0.15) near the time of flight corresponding to maximum dynamic pressure. The lowest flexible body mode frequency is just over 1 cycle per second.

The engine dynamics were approximated by the following transfer function

$$\frac{\beta(s)}{\beta_c(s)} = \frac{27{,}000}{(s + 30)(s^2 + 18s + 900)}$$

which neglects engine inertia. In addition, the angular deflection and rate of the engine were limited. The deflection limit was not exceeded during the course of the study while the rate limit was exceeded only in extreme cases.

Instrument panel details are shown in figure 5. The two large instruments are standard aircraft all-attitude indicators, with the upper one being used as the primary flight instrument except during high dynamic pressure flight. The upper indicator is rotated clockwise 90° from the standard aircraft orientation to simulate the gimbal order that would be used for the spacecraft. Vehicle attitude is displayed on the sphere of this indicator with pitch and yaw attitude errors being presented on the flight director needles. Scaling on the needles was 10° attitude error per inch. During the high dynamic pressure region of flight the lower all-attitude indicator was the primary instrument. Attitude error is presented on the sphere of this indicator while the pitch and yaw body-mounted normal accelerometer outputs are displayed on the flight director needles and are scaled 1/8 g per inch. Vehicle attitude rates (driven by spacecraft sensors) are presented on the three d.c. meters at the upper right of the display panel. A 45° meter deflection corresponded to a 4° per second vehicle attitude rate. The instrument to the left of the upper all-attitude indicator was used as a clock.

A two-axis side-arm "pencil" controller and rudder pedals were used early in the study but the three-axis side-arm controller shown in figure 6 was used for the majority of the study. Stick force and displacement characteristics for this controller are shown in figure 7. Performance comparisons showed little difference in changing the controller.

Fixed Cockpit and Centrifuge

The fixed-cockpit simulator used is shown in figure 8. Figure 9 shows the Ames five-degrees-of-freedom centrifuge which has a maximum capability of 6 g. Vibration levels and response of the centrifuge are discussed in the Results and Discussion section of the report.

Simulation Equations

The rigid body equations of motion simulated were a perturbation set with respect to a reference frame moving along the nominal trajectory.

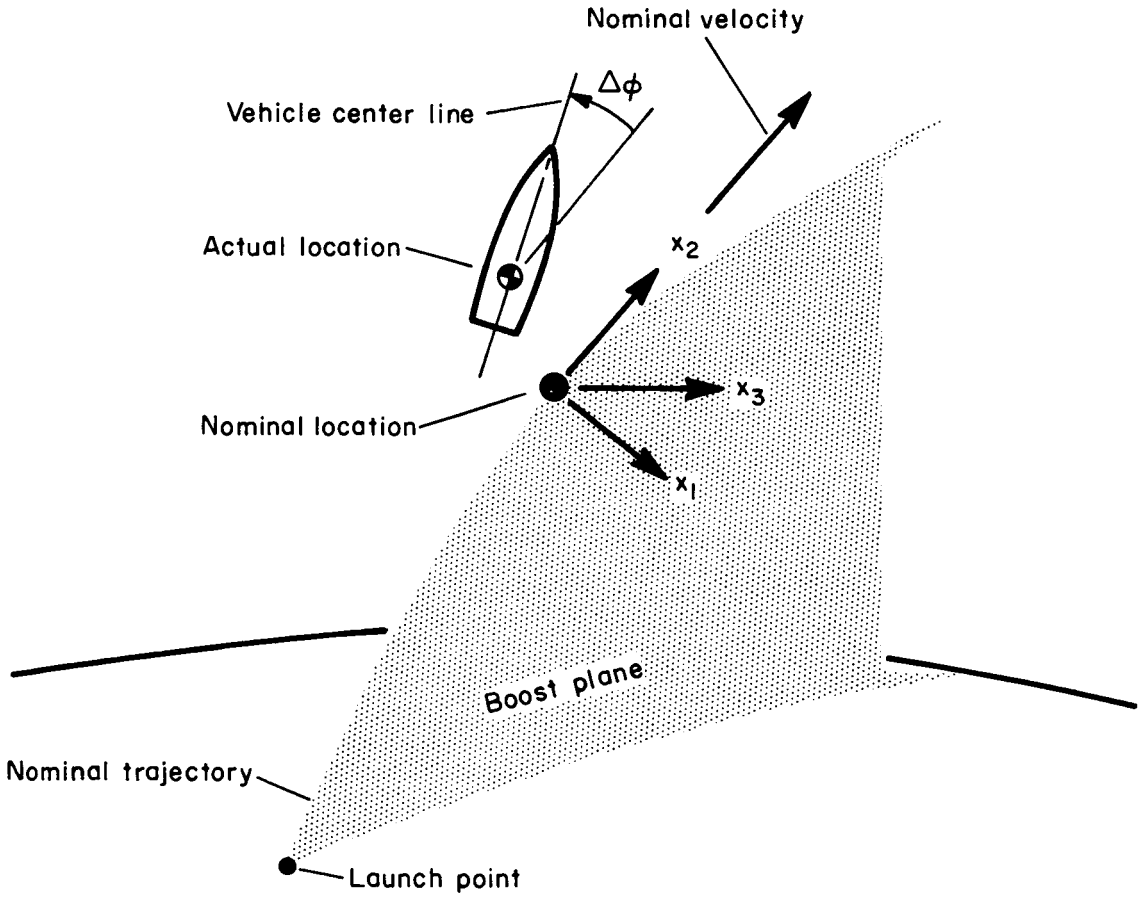

Axes x_1, x_2, x_3 form a right-hand orthogonal system with x_2 alined along the nominal velocity vector, and axes x_1, x_2 lying in the nominal boost plane. The dynamics of the first stage propellants (two tanks) and up to two structural elastic modes were included. The linearized, time varying coefficient equations of motion are given below:

Rigid body (including the ith tank):

$$\ddot{x}_3 = F_\alpha \alpha_Y + F_\varphi \Delta\varphi_Y^* + F_\beta \beta_Y + \sum_i \frac{m_{si}}{m} \left(\omega_{si}^2 \xi_{3i} + 2\zeta_{si}\omega_{si}\dot{\xi}_{3i} \right) \tag{1}$$

$$\ddot{x}_1 = -F_\alpha \alpha_P - F_\varphi \Delta\varphi_P^* - F_\beta \beta_P + \sum_i \frac{m_{si}}{m} \left(\omega_{si}^2 \xi_{1i} + 2\zeta_{si}\omega_{si}\dot{\xi}_{1i} \right) \tag{2}$$

$$\Delta\ddot{\varphi}_Y^* = M_\alpha \alpha_Y - M_\beta \beta_Y - \sum_i \frac{57.3 m_{si}}{I} \left[\left(x_{si}\omega_{si}^2 - 57.3 F_\varphi \right) \xi_{3i} + x_{si}\left(2\zeta_{si}\omega_{si} \right) \dot{\xi}_{3i} \right] \quad (3)$$

$$\Delta\ddot{\varphi}_R^* = -M_\beta' \beta_R \quad (4)$$

$$\Delta\ddot{\varphi}_P^* = M_\alpha \alpha_P - M_\beta \beta_P + \sum_i \frac{57.3 m_{si}}{I} \left[\left(x_{si}\omega_{si}^2 - 57.3 F_\varphi \right) \xi_{1i} + x_{si}\left(2\zeta_{si}\omega_{si} \right) \dot{\xi}_{1i} \right] \quad (5)$$

$$\ddot{\xi}_{3i} + 2\zeta_{si}\omega_{si}\dot{\xi}_{3i} + \omega_{si}^2 \xi_{3i} = \frac{x_{si}}{57.3} \Delta\ddot{\varphi}_Y^* - \ddot{x}_3 + F_\varphi \Delta\varphi_Y^* \quad (6)$$

$$\ddot{\xi}_{1i} + 2\zeta_{si}\omega_{si}\dot{\xi}_{1i} + \omega_{si}^2 \xi_{1i} = -\frac{x_{si}}{57.3} \Delta\ddot{\varphi}_P^* - \ddot{x}_1 - F_\varphi \Delta\varphi_P^* \quad (7)$$

$$\alpha_Y = \Delta\varphi_Y^* + \alpha_{w_Y} - \frac{57.3}{V} \dot{x}_3 \quad (8)$$

$$\alpha_P = \Delta\varphi_P^* + \alpha_{w_P} + \frac{57.3}{V} \dot{x}_1 \quad (9)$$

$$\ddot{\gamma}_3^* = F_\alpha \alpha_Y + F_\beta \beta_Y + \frac{l_a}{57.3} \Delta\ddot{\varphi}_Y^* \quad (10)$$

$$\ddot{\gamma}_1^* = -F_\alpha \alpha_P - F_\beta \beta_P - \frac{l_a}{57.3} \Delta\ddot{\varphi}_P^* \quad (11)$$

Elastic body (ith mode):

$$\ddot{\eta}_{3i} + 2\zeta_{b_i}\omega_{b_i}\dot{\eta}_{3i} + \omega_{b_i}^2 \eta_{3i} = K_{1i}\beta_Y + K_{2i}\ddot{\beta}_Y \quad (12)$$

$$\ddot{\eta}_{2i} + 2\zeta_{b_i}\omega_{b_i}\dot{\eta}_{2i} + \omega_{b_i}^2 \eta_{2i} = K_{1i}\beta_P + K_{2i}\ddot{\beta}_P \quad (13)$$

Pilot display and control system parameters:

$$\Delta\varphi_Y = \Delta\varphi_Y^* + \sum_i K_{3i}\eta_{3i} \quad (14)$$

$$\Delta\varphi_R = \Delta\varphi_R^* \tag{15}$$

$$\Delta\varphi_P = \Delta\varphi_P^* + \sum_i K_{3i}\eta_{2i} \tag{16}$$

$$\dot{\varphi}_Y = \Delta\dot{\varphi}_Y^* + \sum_i K_{4i}\dot{\eta}_{3i} \tag{17}$$

$$\dot{\varphi}_R = \Delta\dot{\varphi}_R^* + \dot{\chi}_R \tag{18}$$

$$\dot{\varphi}_P = \Delta\dot{\varphi}_P^* + \sum_i K_{4i}\dot{\eta}_{2i} + \dot{\chi}_P \tag{19}$$

$$\varphi_Y = \Delta\varphi_Y \tag{20}$$

$$\varphi_R = \Delta\varphi_R + \chi_R \tag{21}$$

$$\varphi_P = \Delta\varphi_P + \chi_P \tag{22}$$

$$\ddot{\gamma}_3 = \ddot{\gamma}_3^* + \sum_i K_{5i}\ddot{\eta}_{3i} \tag{23}$$

$$\ddot{\gamma}_1 = \ddot{\gamma}_1^* + \sum_i K_{5i}\ddot{\eta}_{2i} \tag{24}$$

The symmetry of the configuration permitted inertia product and aerodynamic coupling to be neglected. Nonlinear terms in the equations of motion were found to have negligible effect for the ranges of perturbations considered.

Time varying coefficient data for representative times of flight are given in table I and bending mode shapes are presented in figure 10.

While many simplifying assumptions were intentionally made in the derivation of these equations, one inadvertent omission occurred in the equations for the rigid body content of the accelerometer signals, equations (10) and (11). The forces acting between the vehicle and the sloshing masses affect

the accelerometer signal directly as a translational acceleration (terms were omitted) and indirectly through the vehicles angular acceleration (included as $(l_a/57.3)\Delta\ddot{\varphi}^*$ term). With the accelerometer and tank locations used for the study, these two contributions are cancelling in sign. Since the sloshing content of the accelerometer is noise to the pilot in that it obscures the rigid body signal, it is believed that the omission of the direct contribution (making the actually displayed signal larger than it should have been) made the results slightly conservative.

PROCEDURE

The study approach used for investigating the first-stage manual control system consisted of the following phases:

a. Basic handling qualities

b. Bending filter selection

c. Normal mode performance

d. Emergency mode performance

e. System parameter variations

Four Ames research pilots were used for the majority of the simulated flights. Visiting pilots from Edwards Air Force Base and the Manned Spacecraft Center also were used. All simulated flights were conducted as follows: Each pilot flew practice trajectories at a given set of conditions until he felt that he had reached a satisfactory level of familiarity. He then made three simulated flights during which data were collected at the same set of conditions. At the conclusion of the three data runs he rated the configuration (fig. 3).

RESULTS AND DISCUSSION

Basic Handling Qualities

The objective of this portion of the study was to determine the basic control system characteristics for a vehicle of this class. The required stability augmentation, rigid body gain coefficients, and parameters for pilot display were investigated.

A five-degrees-of-freedom rigid body (no fuel sloshing) three-axis, discrete time of flight simulation was used. The discrete time of flight chosen was that corresponding to maximum dynamic pressure. Since the maximum steady-state wind and maximum wind shear both occur near this time of flight, it was felt, and later justified, that this would be the critical design point of the trajectory. The wind disturbance used was similar to that shown

in figure 2, but was idealized to a ramp input building from 0 to 75 meters per second at a rate of 10 meters per second per second. The direction of this wind was randomly rotated between each piloted run. The piloted runs were approximately 30 seconds to 1 minute in duration, with the ramp wind disturbance commencing some random time after the run was initiated.

The pilot task was to minimize the rigid-body bending moment, while stabilizing the roll attitude, in the presence of the wind disturbance. As discussed in the design constraints section, aerodynamic angle of attack and engine gimbal angle both contribute to the rigid-body bending moment. The pilot therefore attempted to zero the angle of attack (turning the vehicle into the relative wind) by utilizing the body-mounted accelerometer signals displayed on the flight director needles, while minimizing engine gimbal angles by making the minimum required controller inputs. Experience indicated the proper magnitude of controller input necessary. This task is more difficult than attitude stabilization alone, as it requires maneuvering the vehicle through several degrees of attitude change.

If fuel sloshing and engine dynamics are neglected and rate augmentation assumed, the rigid-body equations for the yaw channel become:

$$\ddot{x} = F_\alpha \alpha + F_\varphi \Delta\varphi^* + F_\beta \beta$$

$$\Delta\ddot{\varphi}^* = M_\alpha \alpha - M_\beta \beta$$

$$\alpha = \Delta\varphi^* + \alpha_w - \frac{57.3}{V}\dot{x}$$

$$\beta = a_1 \Delta\dot{\varphi}^*$$

where the yaw subscript has been dropped. If the time varying coefficients of this system of equations are assumed to be constant at some time of flight, the characteristic equation of the system is:

$$s\left\{s^2 + \left(M_\beta a_1 + \frac{57.3}{V} F_\alpha\right)s + \left[\frac{57.3 a_1}{V}\left(F_\alpha M_\beta + F_\beta M_\alpha\right) - M_\alpha\right]\right\} = 0$$

Handling qualities were evaluated in terms of the damping ($2\zeta\omega_n$) and static stability (ω_n^2) of the second order factor of this equation, where

$$2\zeta\omega_n = M_\beta a_1 + \frac{57.3}{V} F_\alpha$$

$$\omega_n^2 = \frac{57.3 a_1}{V}\left(F_\alpha M_\beta + F_\beta M_\alpha\right) - M_\alpha$$

The aerodynamic static stability term, M_α, is the predominant term in ω_n^2 and is normally of small magnitude for the Saturn V, approaching a maximum value of -0.142 at maximum dynamic pressure. With this low value of instability, previous research indicated (see ref. 7) that it could be satisfactorily controlled with rate augmentation only.

For this case, as seen in figure 4, there are only two gains per channel to choose in the control system design if the pilot's display and controller are assumed to be satisfactory. These are the rate loop gain coefficient and the pilot's controller sensitivity. Figures 11 and 12 present pilot rating and maximum rigid-body bending moment, respectively, as a function of these two parameters. The abscissas represent controller sensitivity presented as the maximum angular acceleration obtainable with full controller deflection. The ordinate represents system damping, $2\zeta\omega_n$, seen in the equation above to vary linearly with rate gain, a_1. The parameter values were varied simultaneously in the pitch and yaw channel. The rate loop gain coefficient in the roll channel was set to correspond to a time constant of about one second, while the roll channel controller sensitivity was fixed at about $15^\circ/sec^2$ maximum roll control power.

The significant result shown is the insensitivity of bending moment performance to the two parameters. Nominal values of damping and controller sensitivity chosen are indicated. For neutral stability this value of damping gives a time constant slightly over 1 second. Because of the dependence of rigid-body bending moment on engine gimbal angle, the best bending moment performance occurred at controller sensitivities slightly lower than that best for pilot rating. At still lower controller sensitivities the vehicle becomes uncontrollable because of the pilot's inability to command sufficient engine angle to overcome the wind disturbance uprighting torque. At higher values the controller is overly sensitive. Although the figures indicate that control is possible with no rate augmentation, it must be recalled that the simulation was highly idealized.

For the data in figures 11 and 12 the body-mounted accelerometers were mounted at the vehicle's "instantaneous" center of rotation. This was defined as that location on the longitudinal axis about which the vehicle rotates when an engine is deflected and no aerodynamic force is present. At this location (about 15 meters forward of the vehicle's center of gravity at maximum dynamic pressure) the accelerometer signal due to vehicle rotational acceleration resulting from an engine deflection is exactly cancelled by the accelerometer signal due to vehicle translational acceleration. When an aerodynamic force is present then, the only accelerometer signal present will be that due to the aerodynamic force. This may be seen by combining rigid-body equations (5) and (11), neglecting sloshing, to give the accelerometer signal in terms of angle of attack and engine gimbal angle.

$$\gamma^* = -\left(F_\alpha + \frac{l_a}{57.3} M_\alpha\right)\alpha - \left(F_\beta - \frac{l_a}{57.3} M_\beta\right)\beta$$

For the instantaneous center of rotation (no β contribution) the accelerometer location, l_a, is:

$$l_a = 57.3 \frac{F_\beta}{M_\beta}$$

The accelerometer signal is then proportional to α. Figure 13 shows the effect on pilot opinion and bending moment of moving the accelerometer from this location. The abscissa represents longitudinal location of the accelerometer forward of the c.g., normalized to the distance to the instantaneous center of rotation. In the equation for γ^* above, changing l_a from the value for the instantaneous center of rotation will cause the coefficient of the β term to be either positive or negative. When the accelerometer is moved aft of the center of rotation, vehicle translational acceleration predominates, causing a very confusing signal for attitude control. Consequently, the performance as shown in figure 13 deteriorated rapidly. Moving the accelerometer forward causes the rotational acceleration component of the signal to predominate which provides a signal that tends to reduce angular accelerations (acceleration lead) and is not nearly so confusing for attitude control. The figure shows that the performance is relatively insensitive to accelerometer location over a range of about 15 meters and then deteriorates slowly. Since the center of rotation moves with time of flight, the nominal value for the remainder of the study was chosen so that the accelerometer remained slightly forward of the instantaneous center of rotation (1.0 to 1.25 in figure 13) during the high dynamic pressure region and is physically located at station 2000 in figure 1.

To verify the assumption that a "rate augmentation only" system would not cause large decrements in performance as compared with more complex augmentation, an accelerometer loop was added to the control system of figure 4. The augmentation system signal to the engine then becomes

$$\beta = a_1 \Delta\dot{\varphi}^* + g_2 \ddot{\gamma}^*$$

where g_2 is the loop gain coefficient. If the accelerometer is located near the instantaneous center of rotation, it can be seen from the equation for γ^* above that the engine signal becomes

$$\beta = a_1 \Delta\dot{\varphi}^* - g_2 \left(F_\alpha + \frac{F_\beta}{M_\beta} M_\alpha \right) \alpha$$

This augmentation signal leads to the following expressions for system damping and stability:

$$2\zeta\omega_n = M_\beta a_1 + \frac{57.3}{V} F_\alpha + g_2 \frac{57.3}{V} F_\beta \left(F_\alpha + \frac{F_\beta M_\alpha}{M_\beta} \right)$$

$$\omega_n^2 = \left(\frac{57.3 a_1}{V} + g_2 \right) \left(M_\beta F_\alpha + F_\beta M_\alpha \right) - M_\alpha$$

Figure 14 shows bending moment performance and pilot rating as a function of ω_n^2.

Since the accelerometer loop gain coefficient has a negligible effect on $2\zeta\omega_n$, and a_1 was maintained at the nominal value of 0.75, $2\zeta\omega_n$ was essentially constant. Increasing the stability had little effect on bending moment performance, but since the pilot's task of nulling the accelerometer is eased, the pilot rating improves. However, because bending moments were not reduced with the increased stability, it was felt that the added complexity of accelerometer augmentation (especially considering elastic body and fuel-sloshing effects) was not justified.

Figure 15 summarizes the work on handling qualities and compares the present results with those of reference 7. Pilot opinion boundaries are presented as a function of system damping and stability. The satisfactory area corresponds to a pilot rating of 3.5 or less. The acceptable for normal operation area corresponds to pilot ratings between 3.5 and 4.5 while the emergency operation area was for pilot ratings between 4.5 and 6.5. The unaugmented vehicle and recommended augmentation points are indicated. The pilot task for the flight controllability limit of reference 7, shown in figure 15, was to maintain vehicle angle of attack at less than 2° with no disturbances while the pilot's task for the present results, as discussed earlier, was to minimize the rigid body bending moment in the presence of a severe wind disturbance. The present task required that the pilot rotate the vehicle through 5° to 10° of attitude at the wind spike while minimizing the expression used for high q rigid body bending moment (see section on vehicle design constraints)

$$\frac{M}{M_D} = \frac{\alpha}{11} + \frac{\beta}{5}$$

This difference in pilot tasks explains the much more restrictive conditions placed on a Saturn V class vehicle. It should be noted that in the presence of a less severe wind (corresponding to normal operation) the pilot ratings for a given damping and stability level would improve considerably.

Bending Filter Selection

In this phase of the study the filters dictated by the elastic body dynamics were investigated. These included the rate loop augmentation filter, the pilot's controller filter, and the display filters. The discrete time of flight simulation included a single axis, two degrees of rigid body freedom, and two flexible-body modes. It did not include fuel-sloshing dynamics. Other characteristics of the simulation and the pilot task were identical to that used for the basic handling qualities investigation described previously.

Rate augmentation filter.- The rate augmentation filter shown in figure 4 is required to stabilize the elastic structural dynamics present in the closed rate loop. With respect to the Saturn V vehicle, this problem is complicated by the relatively narrow separation of the first bending mode natural

frequency and pilot control frequencies. The design procedure of this filter for a manual attitude control system is, in principle, no different from that normally used for automatic control systems. The procedure involves finding a filter which attenuates or shifts the phase of the bending content of the feedback signals so that adequate stability margins are attained but which does not "significantly" alter the rigid body content of the signals.

With the nominal rate gyro location (station 2470 in fig. 1) a satisfactory rate augmentation filter for the manual control system was determined to be

$$F_1(s) = \frac{336}{(s + 6)(s + 7)(s + 8)}$$

Any system response modes introduced by this filter were heavily damped and not objectionable to the pilot.

Controller filter.- The purpose of this filter is to smooth the output of the pilot's controller at elastic bending frequencies. In conjunction with the augmentation filter described previously, this reduces the magnitude of the structural oscillations. This is important because:

1. The rigid body control task is not obscured at the pilot's displays by elastic oscillations. (Another approach to this problem would smooth the sensor outputs.)

2. The component of bending moment stress due to elastic structural motions is reduced.

3. Motions at the pilot's station caused by elastic motions are reduced. This may be necessary if the motions are severe enough to complicate the pilot's control task.

As seen in figure 4, the phase lags introduced by the controller and any display filters will be additive. Therefore, the introduction of display filters will affect the controller filter design. From item (1) alone, it is not clear what combination of controller and display filters should be used. Items (2) and (3), though, both require the introduction of as much attenuation as is allowable at the controller filter. The best over-all solution, then, is to place the total allowable attenuation and resulting phase lag in the controller filter.

For the present study, a passive second-order filter configuration was chosen for the controller filter.

$$F_2(s) = \frac{\omega_n^2}{s^2 + 2\zeta\omega_n s + \omega_n^2}$$

Piloted simulation runs were made varying the natural frequency, ω_n, of this filter, with a fixed damping ratio, ζ, of 0.5 to produce the results shown in figure 16.

The upper curves of figure 16 show pilot rating and rigid-body bending moment performance, while the lower curve presents the maximum amplitude of the structural elastic motions at the pilot's station for the first and second modes. Lowering the natural frequency of the filter attenuates the pilot's inputs which occur at body elastic frequencies, but the phase lag introduced causes the rigid-body control problem to become more difficult with a corresponding increase in the maximum bending moment and pilot rating. The nominal value indicated in figure 16 was chosen for the remainder of the study.

With these filters and rate gyro location, figure 16 indicates that from a piloted standpoint only the first bending mode is significant, since the elastic motion amplitudes for this mode are much larger than for the second mode. Therefore, it will be the dominant elastic effect seen at the pilot's displays and in his motion cues. Consequently, in later piloted simulations only the first mode was mechanized. It should be recalled, however, that all the structural modes must be included in the study of the rate augmentation filter.

Normal Mode Manual Performance (Fixed Cockpit and Centrifuge)

The performance of the piloted control system described above was investigated on a more realistic simulation. Fuel-sloshing dynamics were investigated as well as the effects of acceleration motion cues on the pilot's control capability. Emphasis was placed on developing pilot techniques to produce the desired performance.

Computer simulation.- The wind disturbance of figure 2 was used while the pitch and yaw channel control system was that of figure 4 with nominal gain values. The roll channel had a simple rate augmentation system with a time constant of 1 second and maximum roll control power of $15^{\circ}/sec^2$. Simulation flights commenced at lift-off and their duration corresponded to the time of flight for the first stage. Strip recordings were made of the significant parameters. A typical run is shown in figure 17. The wind disturbance in this figure, α_w, is the component of angle of attack due to the wind of figure 2.

Initial simulation results were obtained without fuel-sloshing dynamics because the necessary data for simulation were not available. However, as soon as they became available, the effects were investigated. In spite of the low frequencies of oscillation (about 1/2 cps), the addition of fuel-sloshing dynamics caused a negligible decrement in the pilot's ability to control (see discussion of fig. 20). Unless specifically noted, the results of this and subsequent sections include the effects of fuel-sloshing dynamics.

Centrifuge dynamic characteristics.- The ARC centrifuge (fig. 9) used in the study enabled an approximate simulation of the Saturn V, first-stage launch profile to be made. The thrust acceleration (eye balls in) was simulated by rotation of the arm, the three gimbal cab being rotated to aline its longitudinal axis with the resultant g vector. The normal accelerations felt by the pilot during launch caused by rigid body rotation and elastic

body motion were simulated by rotating the cab slightly so there was a small component of the resultant g normal to the cab longitudinal axis. This necessitated making undesired angular accelerations to simulate the linear accelerations. The magnitude of these undesired angular motions at times approached 2 radians/sec^2 and were quite apparent to the pilot although his performance did not suffer noticeably. The frequency response of the cab gimbals was such that less than 20° of phase lag existed at the first elastic structural mode frequency.

The launch vibration profile and any longitudinal oscillations were not simulated directly but a high level of vibration was naturally present in the centrifuge. Root mean square values of vibration reached as high as 0.3 g at frequencies under 20 cps.

In summary, it is felt that the centrifuge provided a conservative simulation of the launch profile. Since the data to be presented show little decrement in performance between the fixed base and centrifuge results, it is concluded that the motion cues present in the Saturn V, S-IC launch profile are not significant for pilot controllability considerations.

Pilot tasks.- Four pilot tasks were evaluated to determine how they affected system performance. The important aspects of each are discussed below.

1. Attitude stabilization: The objective of this task was to control the vehicles attitude to that called for in the open loop guidance program. No attempt was made to reduce loads and the pilot used attitude error as the primary control parameter. Attitude rate and time were also presented.

After lift-off the pilot attempted to zero the pitch and yaw attitude errors while maintaining the correct roll angle. The roll angle program called for a 40° roll commencing at 5 seconds after lift-off and terminating 15 seconds after lift-off at the correct downrange heading. The nominal pitch program then tilted the vehicle into the correct boost plane with the pilot maintaining zero roll angle thereafter. During the wind disturbance time of flight (60 through 90 sec), the pilot must overcome the aerodynamic uprighting torque while maintaining the nominal attitude program. About 5 seconds prior to staging, the pilot let the rate augmentation system null attitude rates in preparation for staging.

2. Load reduction: The objective of this task was to minimize the body bending moment with secondary emphasis being placed on attitude control. As discussed in the section on vehicle constraints, the vehicle structural load or bending moment is a combination of aerodynamic loads and engine induced loads. Since the aerodynamic loads are only significant in the high dynamic pressure region, the recommended piloting procedure utilized the signals from the body-mounted accelerometers as the primary display parameters during this period. The pilot was also presented attitude error, attitude rate, and time.

From lift-off to 60 seconds the piloting technique was similar to that for the attitude stabilization task, the pilot stabilizing the pitch and yaw attitude error signals.

At 60 to 90 seconds his primary emphasis was on nulling the accelerometer signals while maintaining zero roll angle. This was the period during which extreme winds could be expected. From 90 to 105 seconds, he gradually returned to the attitude error signals while maintaining the accelerometer signals at a safe level. After 105 seconds, his procedure was identical to that in the attitude stabilization task. Throughout the flight the pilot minimized the engine induced loads by making smooth, small controller inputs.

3. Trimmer: The objective of this task was to minimize the body bending moment with the pilot trimming a rudimentary automatic guidance system. The automatic system used was the augmentation system of figure 4 with an attitude loop added. The pilot's controller signal was then summed with that of the automatic system. The pilot used the body mounted accelerometer signals as the primary display parameter during the high dynamic pressure time of flight. In addition, attitude error, attitude rate, and time were displayed to the pilot.

From lift-off to 60 seconds the pilot made minor corrections to the automatic system; the attitude augmentation loop stabilized attitude. At 60 to 90 seconds (time for wind disturbance) the pilot acted as an accelerometer loop, attempting to null the accelerometer signals. From 90 to 105 seconds, he gradually let the automatic system regain control. From 105 seconds to staging, he again made minor attitude corrections as necessary to assist the automatic system.

4. No rate augmentation: The objective of this task was to evaluate the pilot's ability to control the vehicle without augmentation. From figure 15 it is seen that this is potentially only an emergency mode of operation. In addition, since the results of figure 15 were for a highly idealized simulation, it was only practically possible to control the vehicle in one axis without augmentation. The pilot was displayed attitude error, attitude rate, time, and body-mounted accelerometer signals.

The pilot attempted to stabilize rate and attitude as well as reduce loads in the yaw axis while an automatic system controlled the pitch and roll axes.

Results and discussion.- Figures 18, 19, and 20 present the primary performance criteria for the four pilot tasks just discussed. Figure 21 shows the magnitude of the fuel-sloshing mass accelerations while figure 22 presents the results of an investigation of the pilot motion cues due to elastic body motions.

As shown in figure 18, the pilots rated the attitude stabilization and trimming tasks acceptable for normal operation (P.R. < 4.5). With the exception of one pilot, all rated the load reduction task as acceptable while generally they rated the no augmentation task acceptable for emergency operation only. The agreement between fixed base and centrifuge results is good.

The structural load during the trajectory was well below the design limit for the load-reduction and trimmer task as shown in figure 19. The maximum

structural loading with the severe wind of figure 2 slightly exceeded the design strength values for the attitude stabilization and no augmentation pilot tasks. The value of bending moment for the attitude stabilization task is similar to that obtained with a typical automatic system with only rate and attitude loops. The centrifuge results, in general, appeared to be slightly higher than the fixed base data. It is felt that this was due to the fairly severe vibration environment of the centrifuge making it impossible to resolve the readings of the display as accurately as the fixed base display.

As discussed in the design constraints section, the data for calculating the contribution to the structural bending moment load of figure 19, due to fuel sloshing, were not available. The magnitude of these sloshing mass accelerations is therefore presented, for reference, in figure 21 as the maximum acceleration in pitch or yaw of either the fuel or liquid oxygen tank propellants during the trajectory. With the low values of accelerations indicated and the mass ratios involved, preliminary data indicate the contribution to structural loading will be small (sloshing contribution to bending moment less than 10 percent of design value).

It has already been noted that the level of sloshing mass accelerations was low enough that their effect on the pilot's control task was negligible. Although a complete investigation of the sloshing problem was not made, it was felt that the location of the tanks close to the vehicle's c.g. prevented more serious problems from arising.

The maximum magnitudes of the elastic body motion cues for either pitch or yaw at the pilot's station are shown in figure 19. The pilot feels them as lateral or normal accelerations superimposed on the longitudinal thrust acceleration. The magnitudes are well below 0.1 g and had no apparent effect on control. To investigate the problem further, the motion cue, due to the elastic motions, was arbitrarily increased by a constant factor to attempt to detect a threshold level. Because of the centrifuge limitations, as discussed previously, this level could only be increased by a factor of 2. This subjected the pilot to lateral and normal accelerations with a maximum value of about 0.2 g. Figure 22 shows that the pilot ratings and structural load values remained unchanged. The pilot was performing the load reduction task.

Trajectory dispersions ranged as high as 3000 meters and 50 m/sec in the attitude stabilization task to as high as 8000 meters and 100 m/sec in the load reduction control task.

Other trajectory parameters of interest may be seen in figure 17 which is the strip recording of a trajectory utilizing the "load reduction" technique. The pilot was controlling all three axes but for convenience only the pitch channel is shown. One parameter of particular interest is the engine gimbal angle. Its low magnitude ($< 1^{o}$) indicates that the thrust vectoring velocity penalty will be negligible.

The results of figures 18 through 22 indicate that a piloted control system can be highly flexible. The pilot may choose to minimize structural load or attitude errors as the situation requires. The results also show

that in an emergency, single-axis control is possible without augmentation. With the severe wind disturbance used (fig. 2), three axis control without augmentation is questionable.

Failure Mode Performance

The effect of the following failure modes was investigated.

1. One engine out
2. Two engines out
3. One engine hard over
4. Rate augmentation out
5. Attitude error display failure
6. Rate augmentation failure during trimmer mode

Since the four outer engines of the S-IC stage all swivel for pitch, yaw, or roll control, the loss of one or more engines severely restricts the capability to control the vehicle. This can be seen readily in the following example sketch where the pilot has called for a pitch maneuver but due to the loss of one engine is also experiencing a roll maneuver.

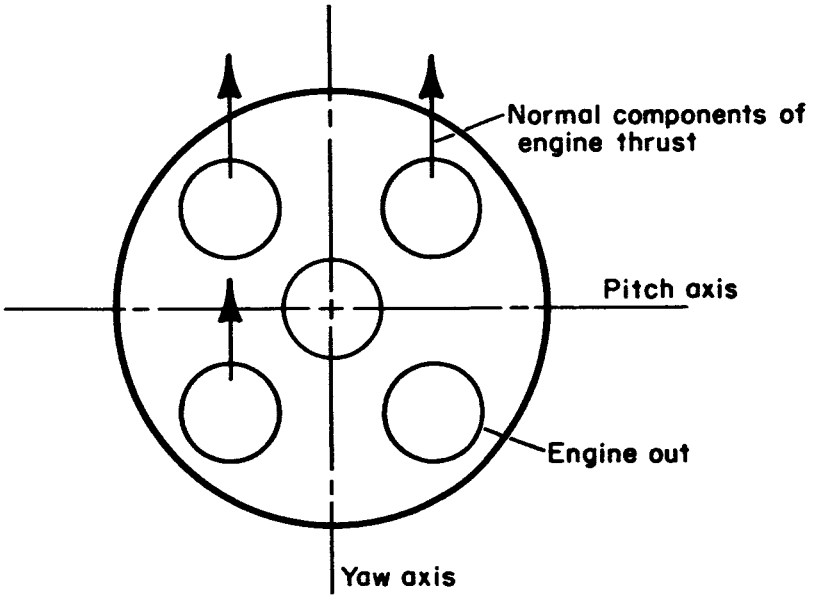

To counteract this unwanted roll torque, the pilot must make a coordinated roll input with the desired pitch input to obtain a pure pitch maneuver. It was found desirable to increase the pilot's roll control power to optimize this task. Figures 23 and 24 present the variation of pilot rating and structural load with maximum roll control power for the three engine failure modes investigated. For these figures the engine or engines were made to fail

at lift-off and the complete trajectory was flown in that mode. The change in trajectory performance in the degree of freedom along the trajectory was not simulated.

Based on these considerations, $75^{o}/sec^{2}$ was chosen as the new nominal value for roll control power as it allowed the pilot to control in the failure mode without affecting normal performance. Roll channel time constant was maintained at 1 second.

Figure 25 presents the results of random time failures for the six failure modes. As mentioned above the change in trajectory performance along the trajectory was not simulated, the primary emphasis being placed on the other five degrees of freedom which constitute the control problem. Three pilots participated in the study, flying at least nine trajectories for each failure mode. A description of the failure modes and pilot techniques, where necessary, is given below.

1. One engine out: engine thrust failure in one of the outer four engines.

2. Two engines out: engine thrust failure in two of the outer four engines on the same side.

3. One engine hard over: pitch or yaw hydraulic actuator on one engine fails, causing engine to swivel to full deflection (5°) in pitch or yaw.

4. Rate augmentation out: rate augmentation failure in one axis of the nominal control system (no attitude or accelerometer loop). Pilot flew remainder of the trajectory with three axis control but with augmentation out in only one axis.

5. Attitude error display failure: The pitch and yaw attitude errors displayed on the flight director needles failed. The pilot utilized a nominal pitch attitude program placed on a scale around the pilot's clock as shown below. By reading the correct value of pitch attitude as a function of time and comparing with the actual value on the all-attitude indicator, the pilot could obtain the pitch attitude error. Since the yaw attitude should be constant during first-stage boost, the pilot controls yaw and roll attitude at the desired values directly from the all-attitude indicator.

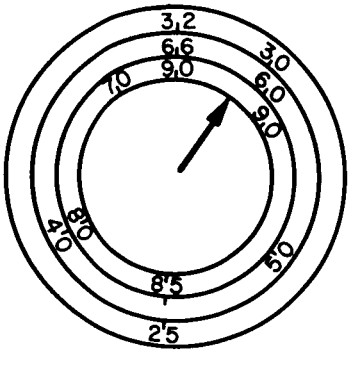

6. Rate augmentation failure during trimmer mode: rate augmentation failed in one axis in the trimmer mode (see section on normal performance).

Because of simulation limitations, the pilot knew what the failure mode would be (not necessarily which axis, etc.), but the time of failure was random. The three columns of figure 25 correspond to the general time of occurrence of the failure: the first column being for nonaerodynamic flight ($0 < t < 60$) prior to high q, the second column

for high q flight ($60 < t < 105$), and the third column for nonaerodynamic flight after high q ($105 < t < 150$). Each circle or cross represents one trajectory. The circles represent satisfactory trajectories while the crosses indicate that one of the three criteria indicated at the bottom of the figure was exceeded either at the time of failure or during the remainder of the flight.

In general, all the failure modes were controllable in the nonaerodynamic flight areas. The performance criteria violations for $0 < t < 60$ generally occurred during subsequent flight in the high q area. One engine out, two engines out, and attitude error failure gave little trouble. The hard over case (severe unbalancing torque of the engine) and the rate augmentation cases were more marginal with the severe wind disturbance used (fig. 2). Rate augmentation out in the trimmer mode was particularly critical. The lag built into the pilot's controller with the controller filter, in conjunction with the neutrally stable system, combined to form an undesirable condition where the pilot tended to amplify the oscillations.

In general, though, even with the wind used (fig. 2) the pilot was quite capable of controlling in the emergency modes investigated. In most cases, it was apparent that the pilot should be able to provide adequate time to decide on alternate modes of action such as continuing with degraded accuracy or initiating a controlled abort.

Vehicle Parameter Variation Study

While it was beyond the scope of the study to analyze in detail the effects of parameter variations, it was felt necessary to examine the sensitivity of system performance (control only) to what was felt were the most important (and carried the least level of confidence) parameters.

Variations were made in: (1) damping of the fuel-sloshing masses, (2) frequency of the first structural elastic mode, and (3) aerodynamic static stability, M_α. The variations were made to the nominal system as described in the preceding two sections and the results are shown in figures 26 through 28.

Figure 26 indicates a small change in the performance criteria shown with the changes in fuel-sloshing damping ratio considered. The rate augmentation system adds damping to this mode of closed-loop system response and the small changes in open-loop damping have little effect on system response.

Because the frequency of the first elastic structural mode is close to pilot control frequencies, it was felt performance might deteriorate rapidly with slightly lower than nominal values. From figure 27 it is seen that even for extreme variations, ±20 percent, the performance decrement is not serious.

Since the nominal control system recommended relied only on rate augmentation, the variation of performance with aerodynamic static stability, M_α, was considered of interest as this is the major contribution to the closed

loop rigid body frequency. The abscissa of figure 28 is presented for high q but the ratio of M_α to nominal M_α was held constant throughout the trajectory. For variations as high as ±100 percent the change in performance is not severe.

From the limited investigation made, it appears that a manual control system is relatively insensitive to system parameter variations.

CONCLUSIONS

A study of the feasibility of manned participation in the control of the first stage of the Saturn V vehicle was conducted. It was concluded that:

1. Pilot participation in the control system provides a high degree of flexibility and may contribute to the successful completion of the control tasks during the first stage of flight.

2. The rate augmentation filter may pose significant design problems because it can add lightly damped system response modes at pilot control frequencies.

3. Single-axis control can be completed without the aid of rate augmentation. For the severe wind disturbance considered three-axis control with no rate augmentation may not be possible.

4. Structural elastic bending motions sensed at the pilot's station are low enough in amplitude that they should not present significant motion cue problems.

5. Fuel-sloshing dynamics do not significantly alter the piloted control problem.

6. A variety of failure modes do not preclude satisfactory control.

7. The piloted control system appears to be relatively insensitive to expected variations in system parameters.

Ames Research Center
National Aeronautics and Space Administration
Moffett Field, Calif., Jan. 13, 1965

REFERENCES

1. Dragseth, G. K.: Feasibility of Piloted Boost Control. The Boeing Co., 1962. Paper presented at TBC Symposium, March 1962.

2. Anon.: ER 11921 - Evaluation of Pilot Manual Control During Boost Flight. The Martin Co., Nov. 1961.

3. Anon.: ER 12378 - Titan III Flight Control System Studies of Human Pilot Capability. Appendix I - The Martin Co., April 1962.

4. Holleman, Euclid C.; Armstrong, Neil A.; and Andrews, William H.: Utilization of the Pilot in the Launch and Injection of a Multistage Orbital Vehicle. IAS paper 60-16.

5. Lukens, David R.; Schmitt, Alfred F.; and Broucek, George T.: Approximate Transfer Functions for Flexible-Booster-and-Autopilot Analysis. WADD TR-61-93, April 1961.

6. Cooper, George E.: Understanding and Interpreting Pilot Opinion. Aero. Engr. Rev., vol. 16, no. 3, March 1957, pp. 47-51, 56.

7. Taylor, Laurence W., Jr.; and Day, Richard E.: Flight Controllability Limits and Related Human Transfer Functions as Determined From Simulator and Flight Tests. NASA TN D-746, 1961.

TABLE I.- VEHICLE CHARACTERISTICS

		Time of flight			Units
		0 (lift-off)	77 (maximum q)	150 (burnout)	Seconds
Rigid body	F_α	0	0.130	0.006	meters/sec^2/deg
	F_β	.17	.30	.70	meters/sec^2/deg
	F_φ	.21	.36	.87	meters/sec^2/deg
	M_α	0	.141	-.016	1/sec^2
	M_β	.84	1.15	3.3	1/sec^2
	M_β'	52.6	52.6	52.6	1/sec^2
	c.g.	1180	1270	1840	inches
	V	0	486	2300	m/sec
	q	0	3650	100	kg/m^2
	χ_R	-40	0	0	deg
	$\dot{\chi}_R$	0	0	0	deg/sec
	χ_P	0	37.0	65.5	deg
	$\dot{\chi}_P$	0	.69	.15	deg/sec
Sloshing	$\frac{m_{s_1}}{m}$	.054	.082	.035	
	$\frac{m_{s_1}}{I}$	.00017	.00018	.000066	1/m^2
	x_{s_1}	16.4	22.9	39.8	meters
	ω_{s_1}	2.15	2.65	3.55	radians/sec
	ζ_{s_1}	.005	.005	.005	
	$\frac{m_{s_2}}{m}$	.075	.121	.070	
	$\frac{m_{s_2}}{I}$	.00023	.00027	.00013	1/m^2
	x_{s_2}	-3.9	6.7	24.9	meters
	ω_{s_2}	2.15	2.70	3.72	radians/sec
	ζ_{s_2}	.005	.005	.005	

TABLE I.- VEHICLE CHARACTERISTICS - Concluded

		Time of flight			Units
		0 (lift-off)	77 (maximum q)	150 (burnout)	Seconds
Bending	ω_{b}	6.77	7.33	8.25	radians/sec
	ζ_{b_1}	.005	.005	.005	
	K_{11}	.46	.46	.46	1/deg-sec^2
	K_{21}	.00077	.00077	.00077	1/deg
	$K_{31}(3260)$	6.94	8.60	4.47	deg
	$K_{41}(2470)$	3.04	2.87	.57	deg
	K_{51}	see figure 10			meters
	ω_{b_2}	11.40	12.30	13.25	radians/sec
	ζ_{b_2}	.005	.005	.005	
	K_{12}	.418	.418	.418	1/deg-sec^2
	K_{22}	.00074	.00074	.00074	1/deg
	$K_{32}(3260)$	-2.98	.86	2.41	deg
	$K_{42}(2470)$	4.59	5.27	3.43	deg
	K_{52}	see figure 10			meters

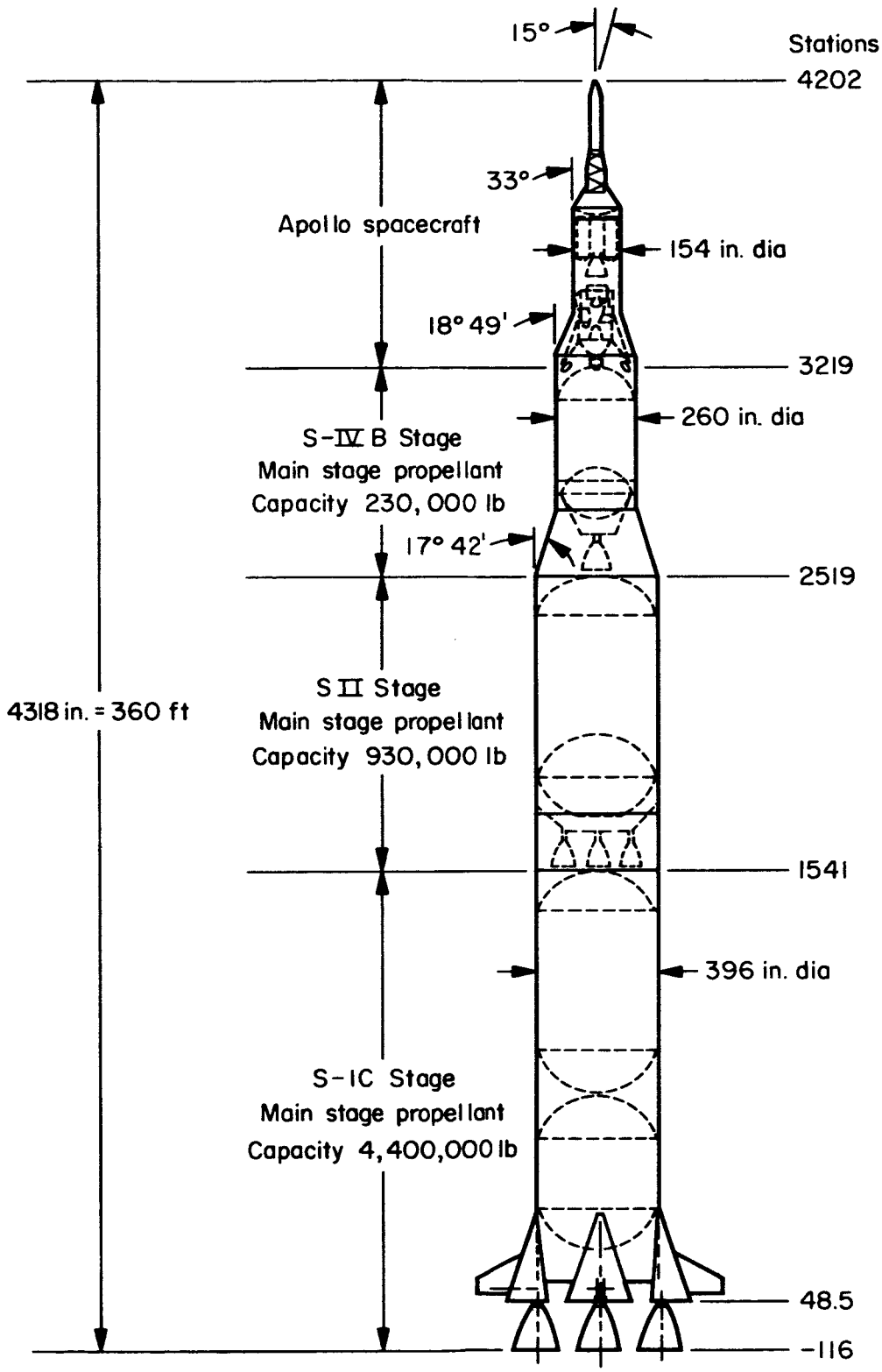

Figure 1.- Saturn V vehicle configuration.

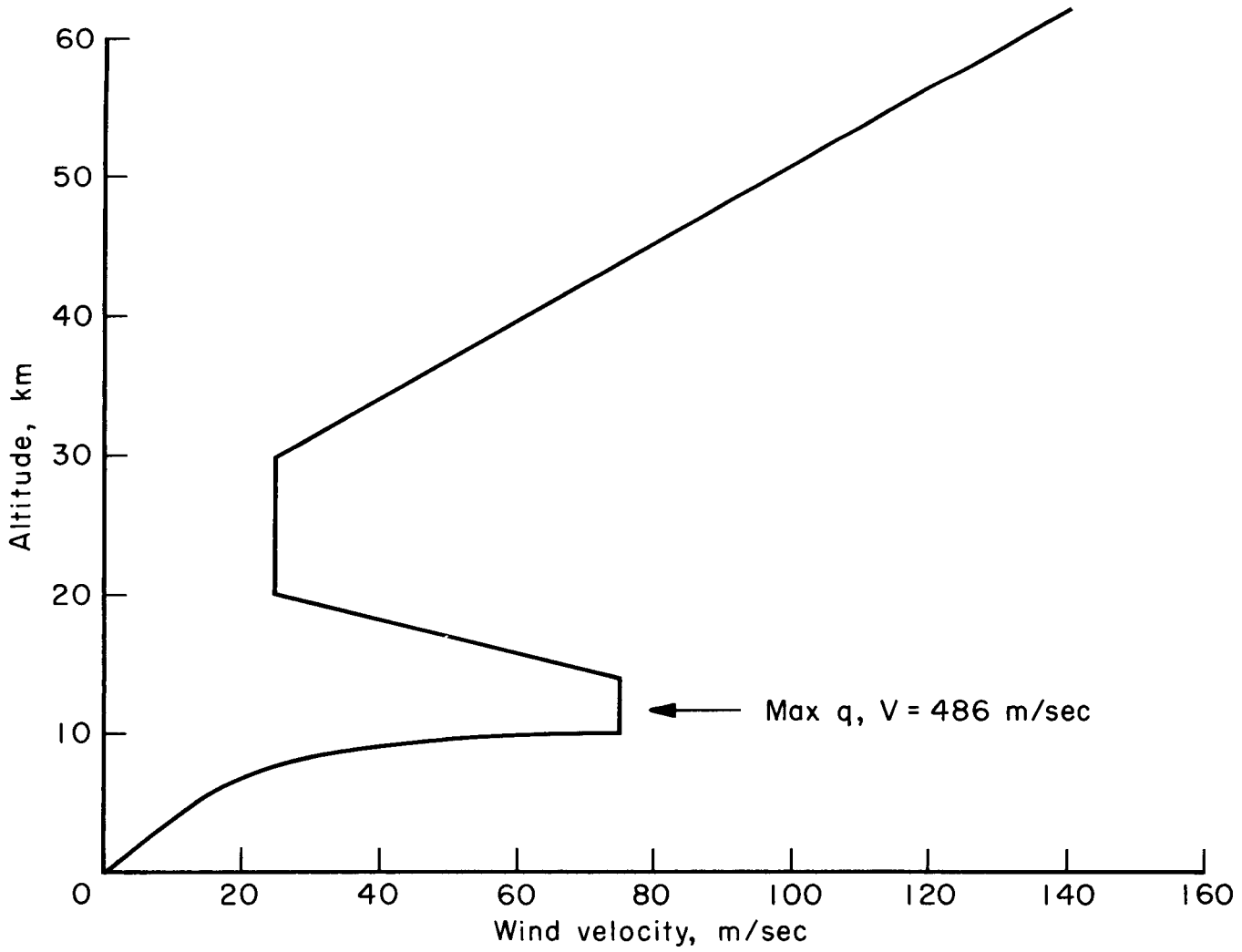

Figure 2.- Wind profile.

PROPOSED PILOT OPINION RATING SYSTEM FOR UNIVERSAL USE

	ADJECTIVE RATING	NUMERICAL RATING	DESCRIPTION	PRIMARY MISSION ACCOMPLISHED?	CAN BE LANDED
NORMAL OPERATION	Satisfactory	1	Excellent, includes optimum	Yes	Yes
		2	Good, pleasant to fly	Yes	Yes
		3	Satisfactory, but with some mildly unpleasant characteristics	Yes	Yes
EMERGENCY OPERATION	Unsatisfactory	4	Acceptable, but with unpleasant characteristics	Yes	Yes
		5	Unacceptable for normal operation	Doubtful	Yes
		6	Acceptable for emergency condition only*	Doubtful	Yes
NO OPERATION	Unacceptable	7	Unacceptable even for emergency condition *	No	Doubtful
		8	Unacceptable - dangerous	No	No
		9	Unacceptable - uncontrollable	No	No

*(Failure of a stability augmenter)

Figure 3.- Rating scale.

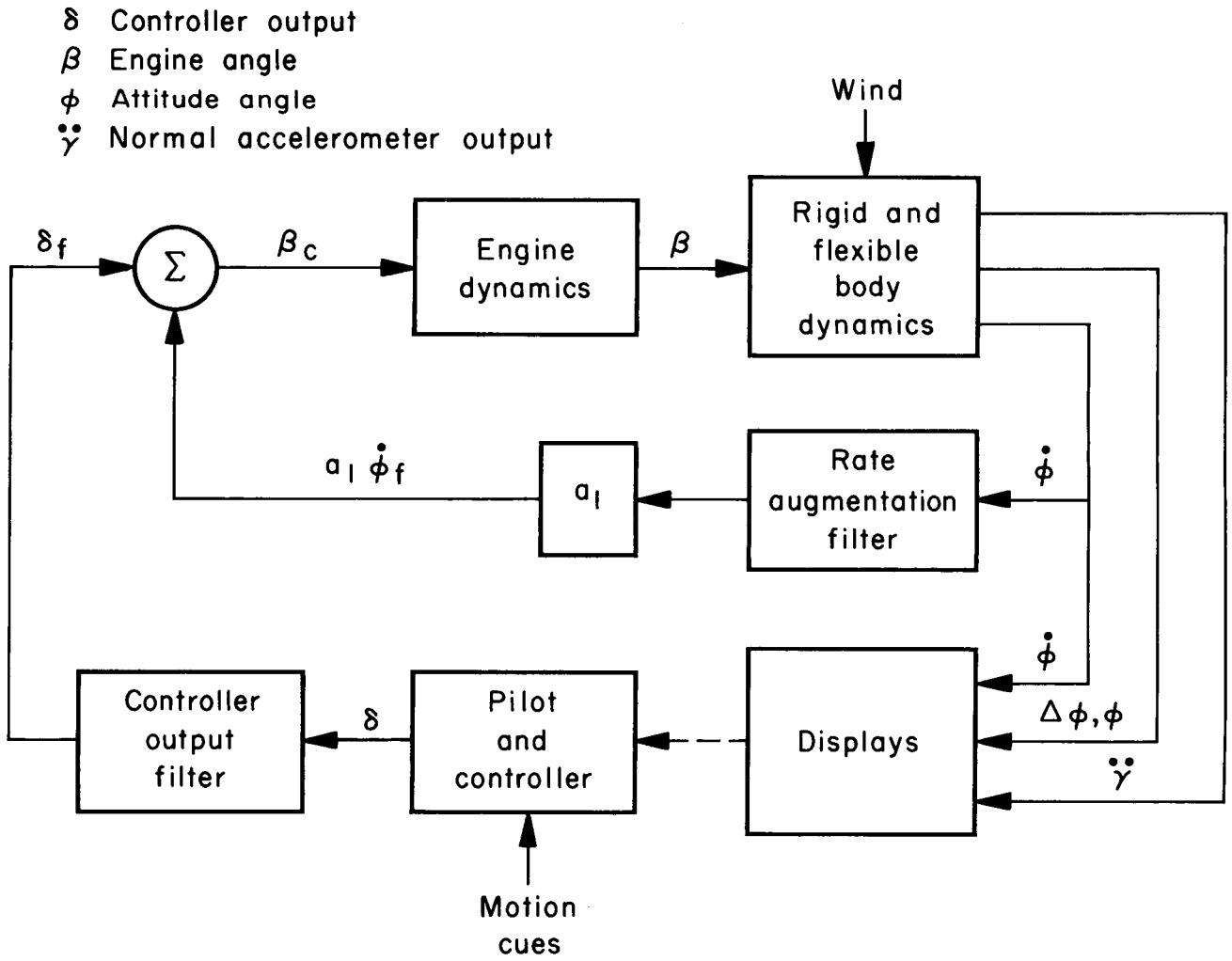

Figure 4.- Pitch, yaw, preliminary primary manual control system.

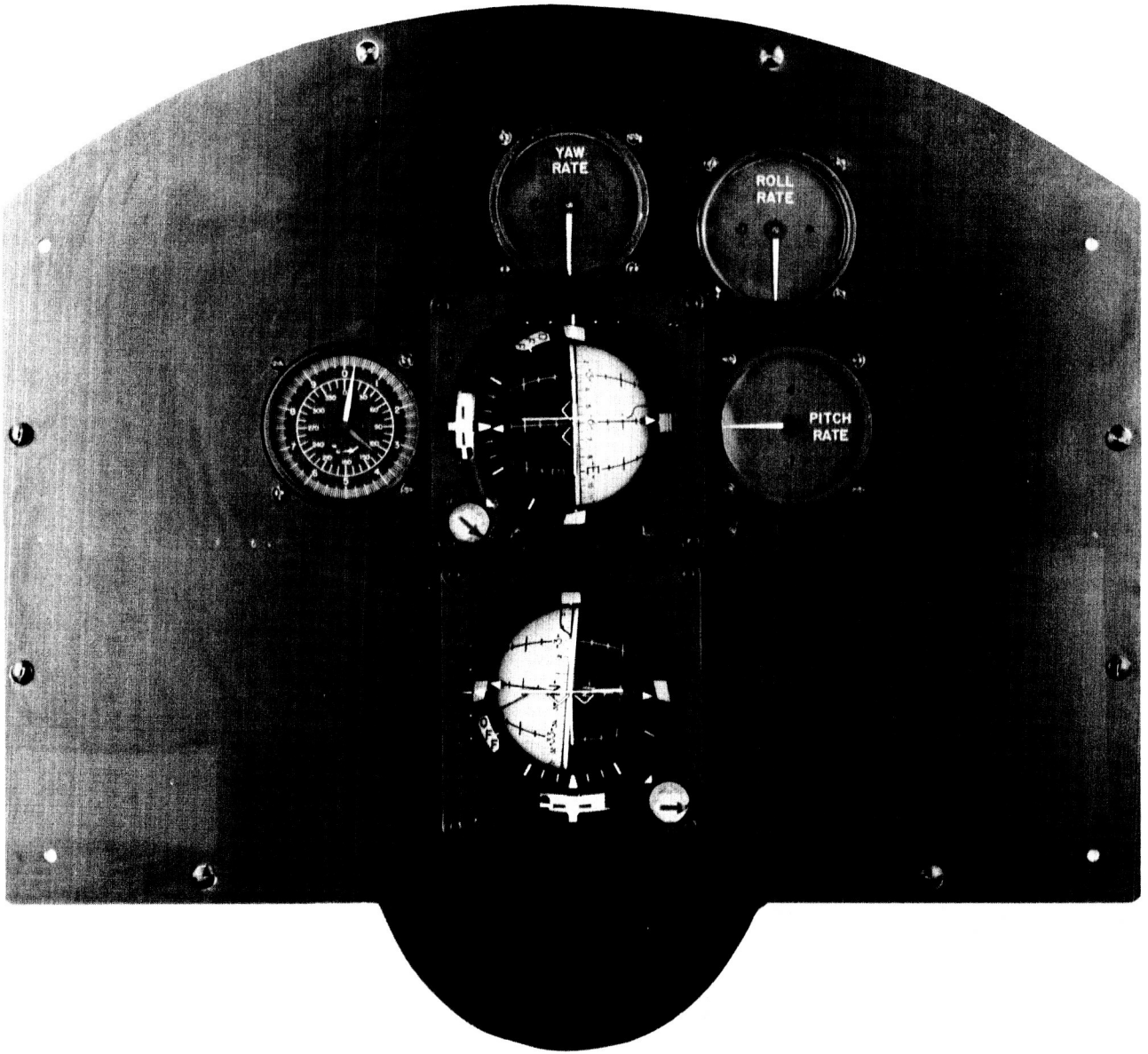

Figure 5.- Pilot display panel.

A-32276

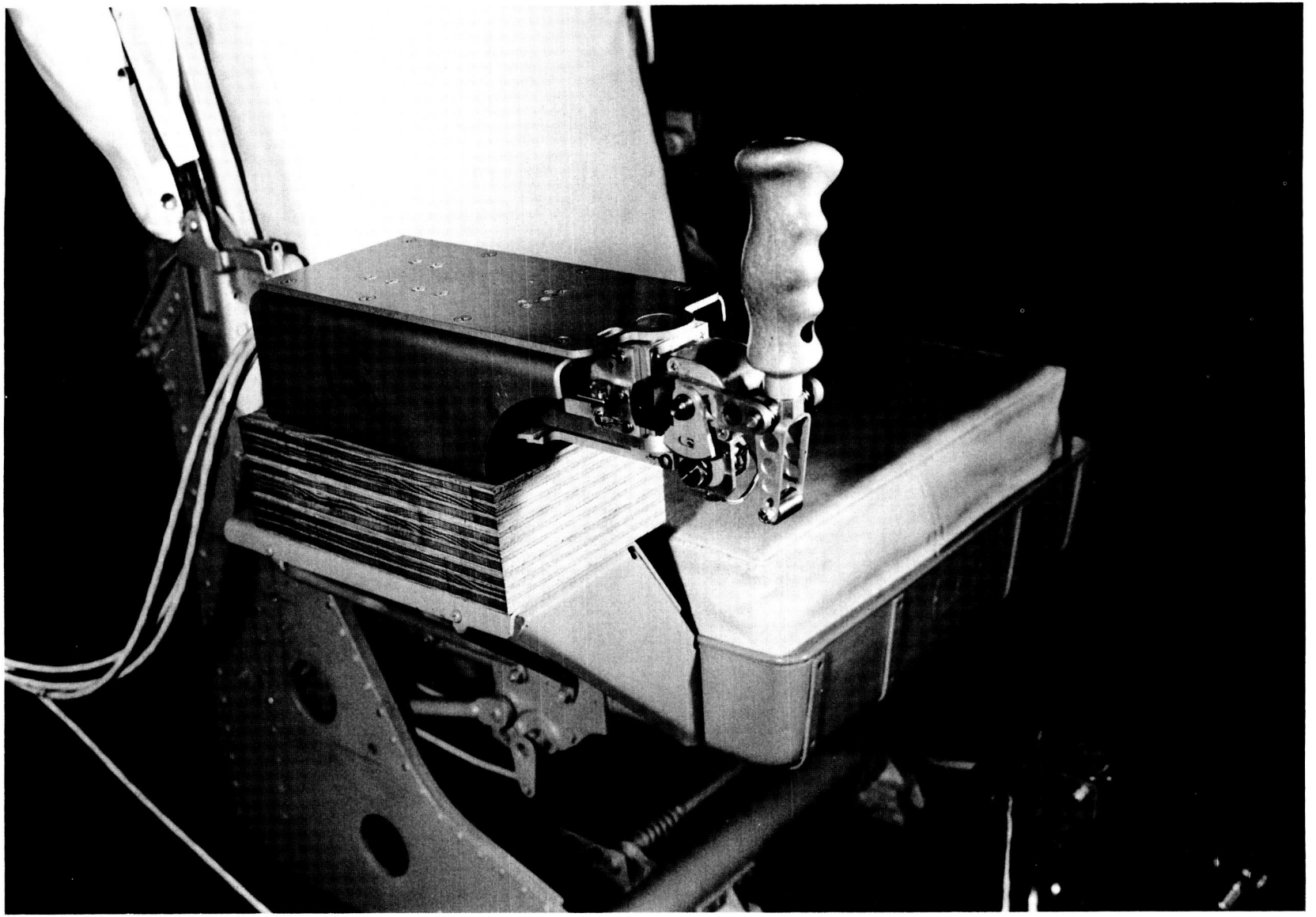

A-31413

Figure 6.- Three-axis side-arm controller.

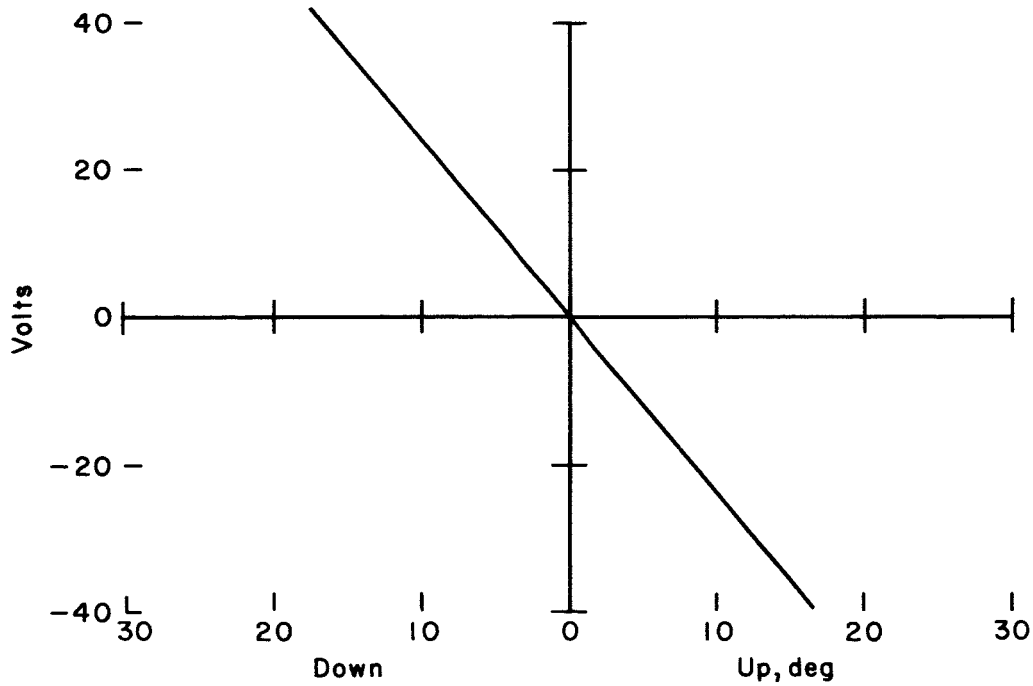

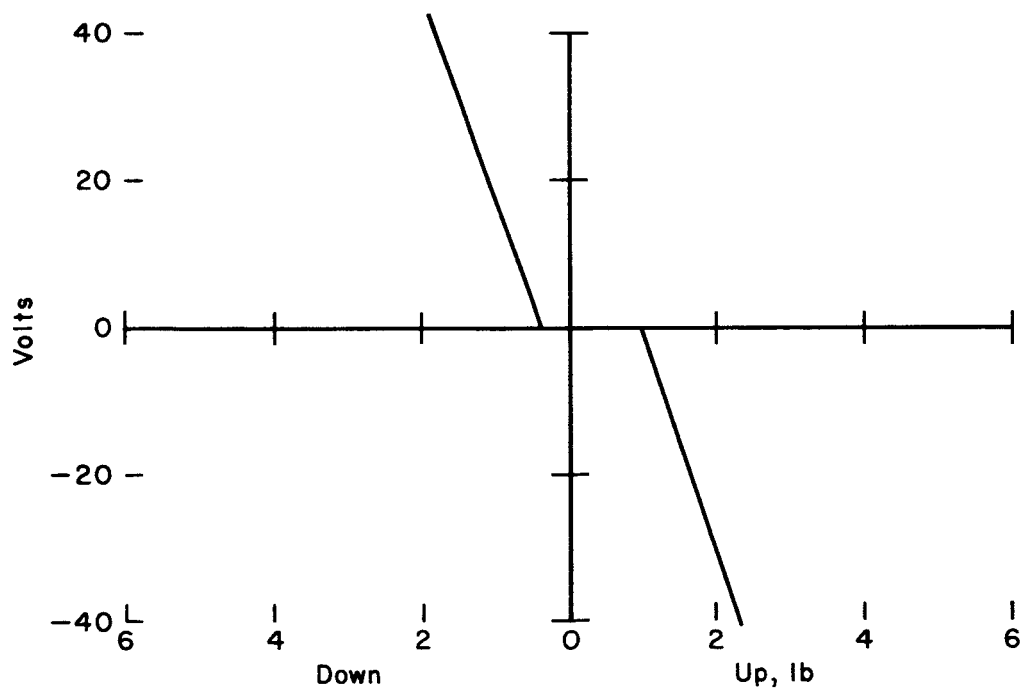

(a) Pitch.

Figure 7.- Three-axis controller characteristics.

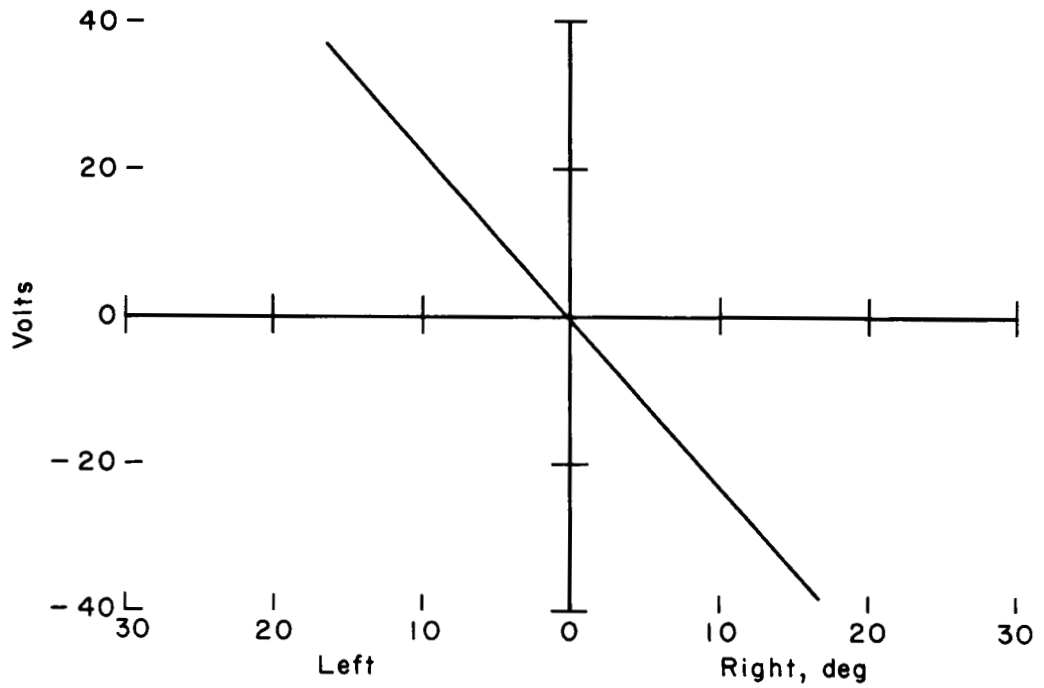

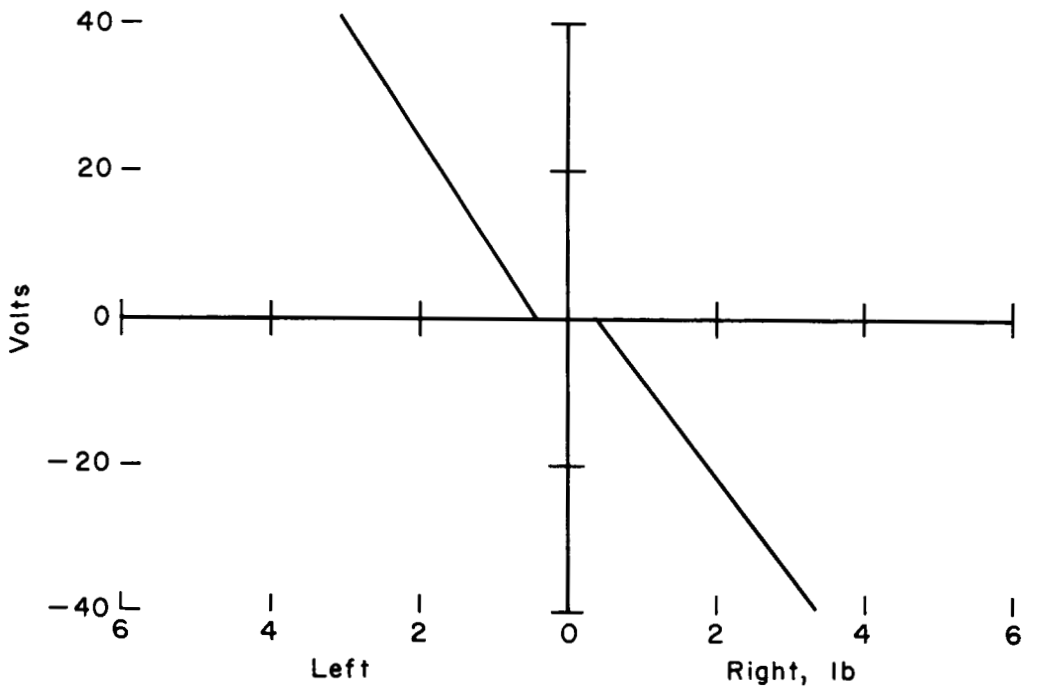

(b) Yaw.

Figure 7.- Continued.

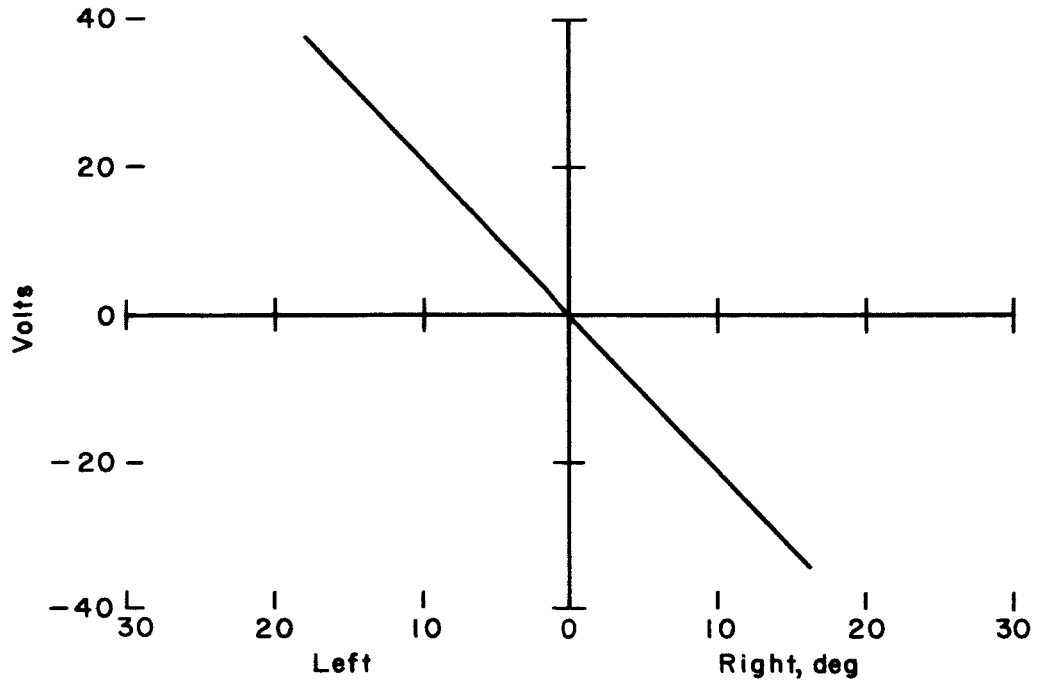

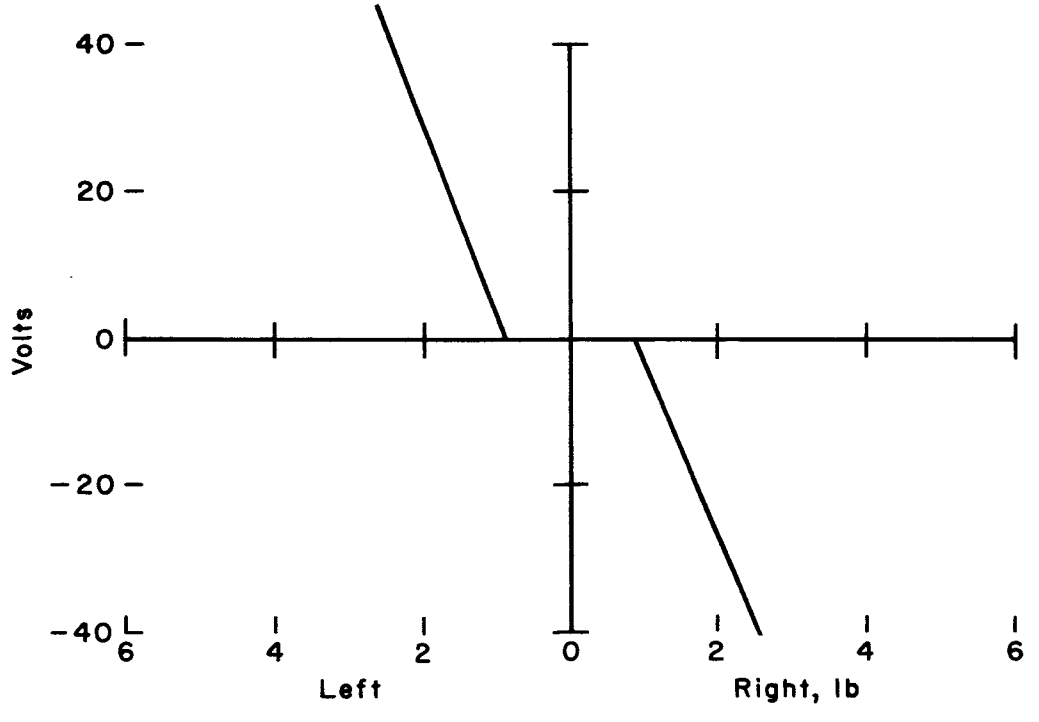

(c) Roll.

Figure 7.- Concluded.

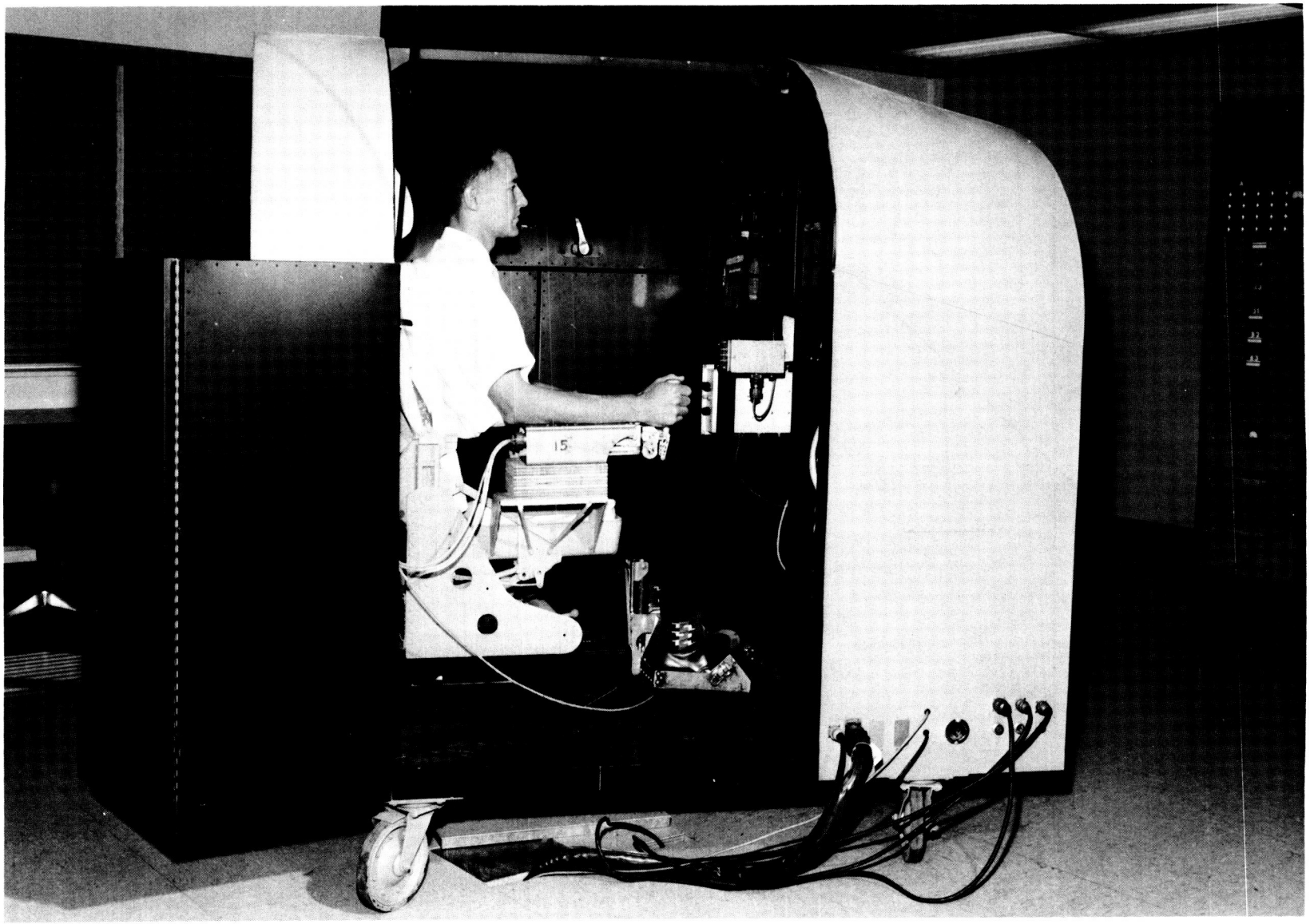

A-31410

Figure 8.- Fixed cockpit simulator.

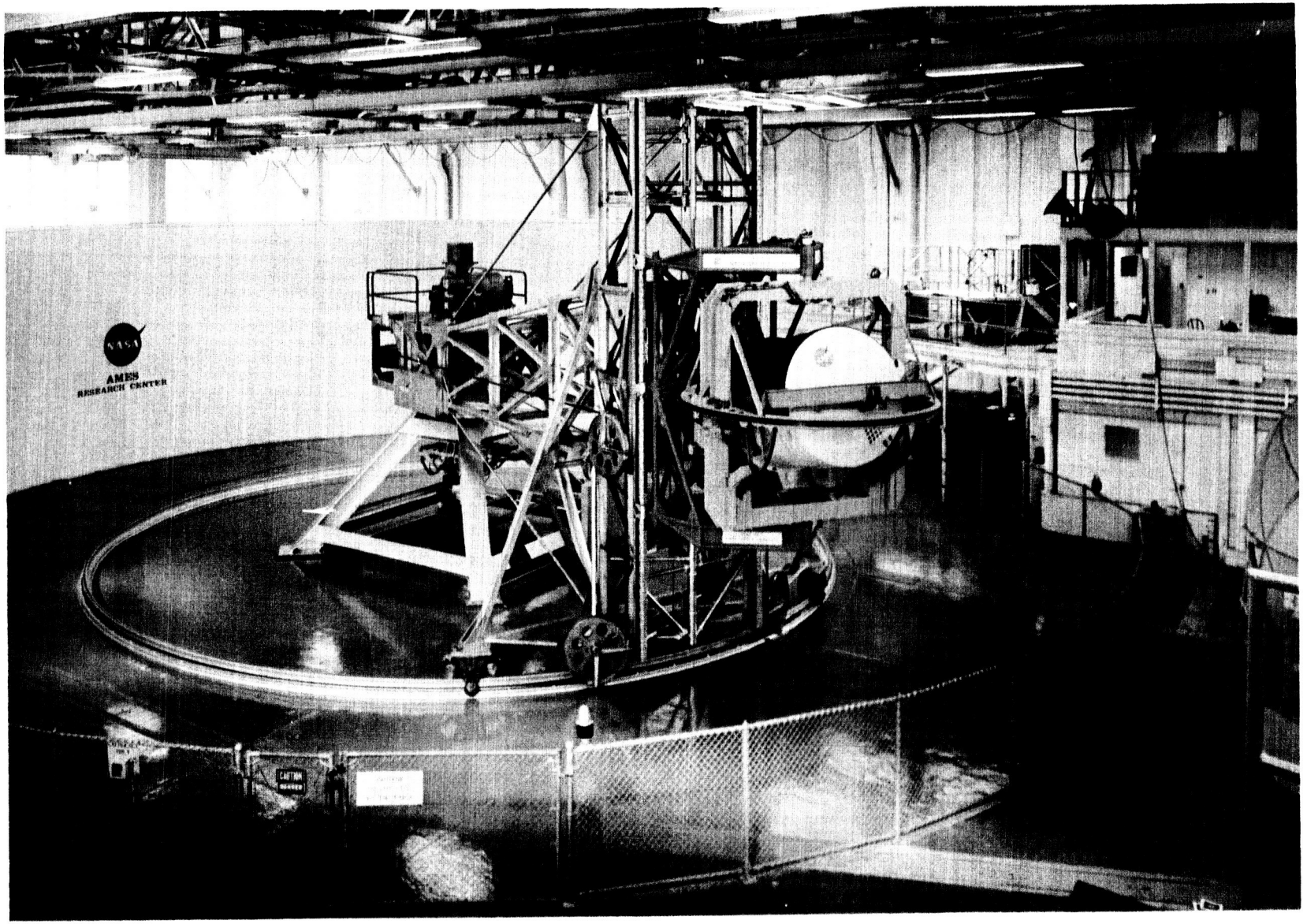

A-31542

Figure 9.- Five-degrees-of-freedom simulator.

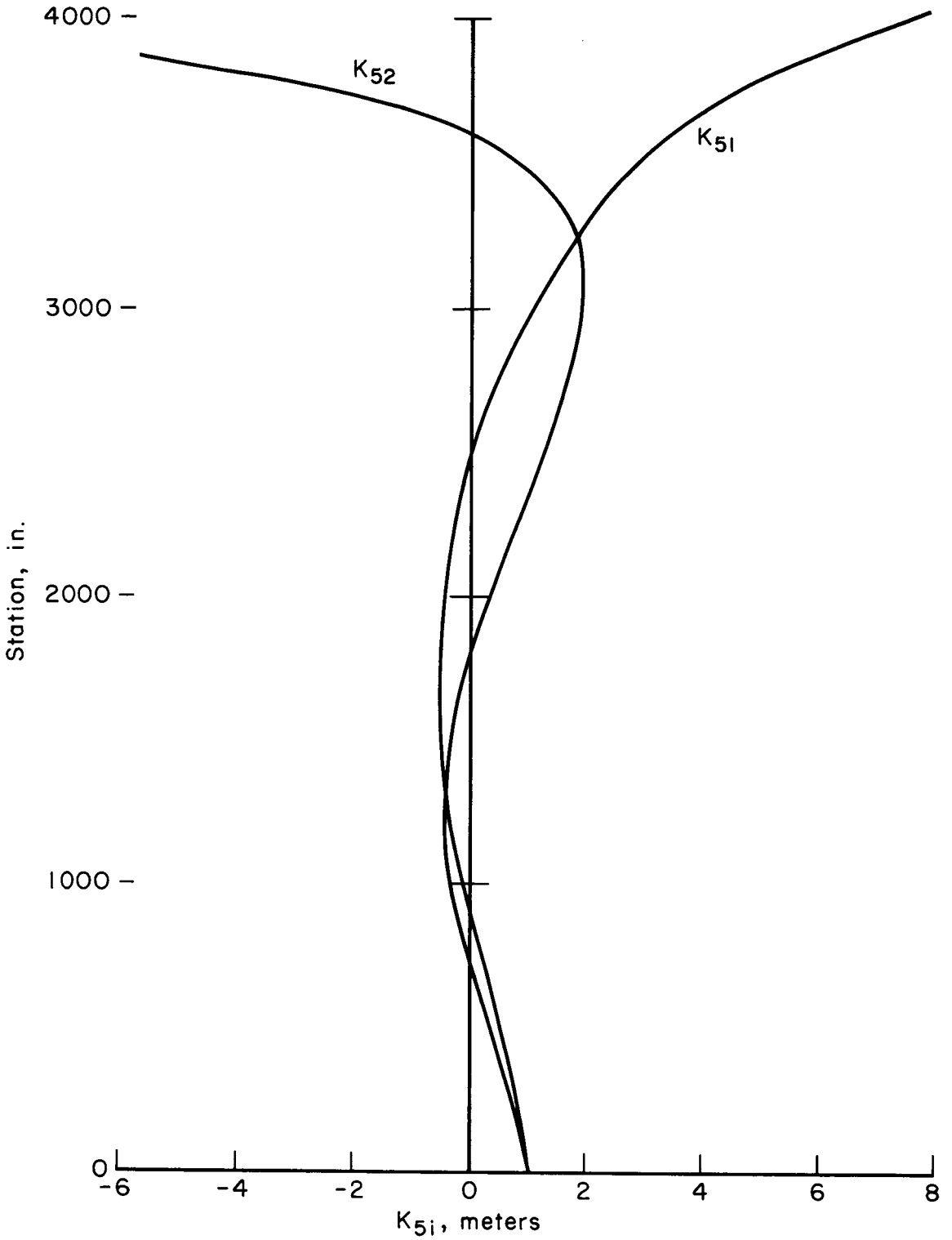

(a) Lift-off (t = 0 sec).

Figure 10.- Bending mode shapes.

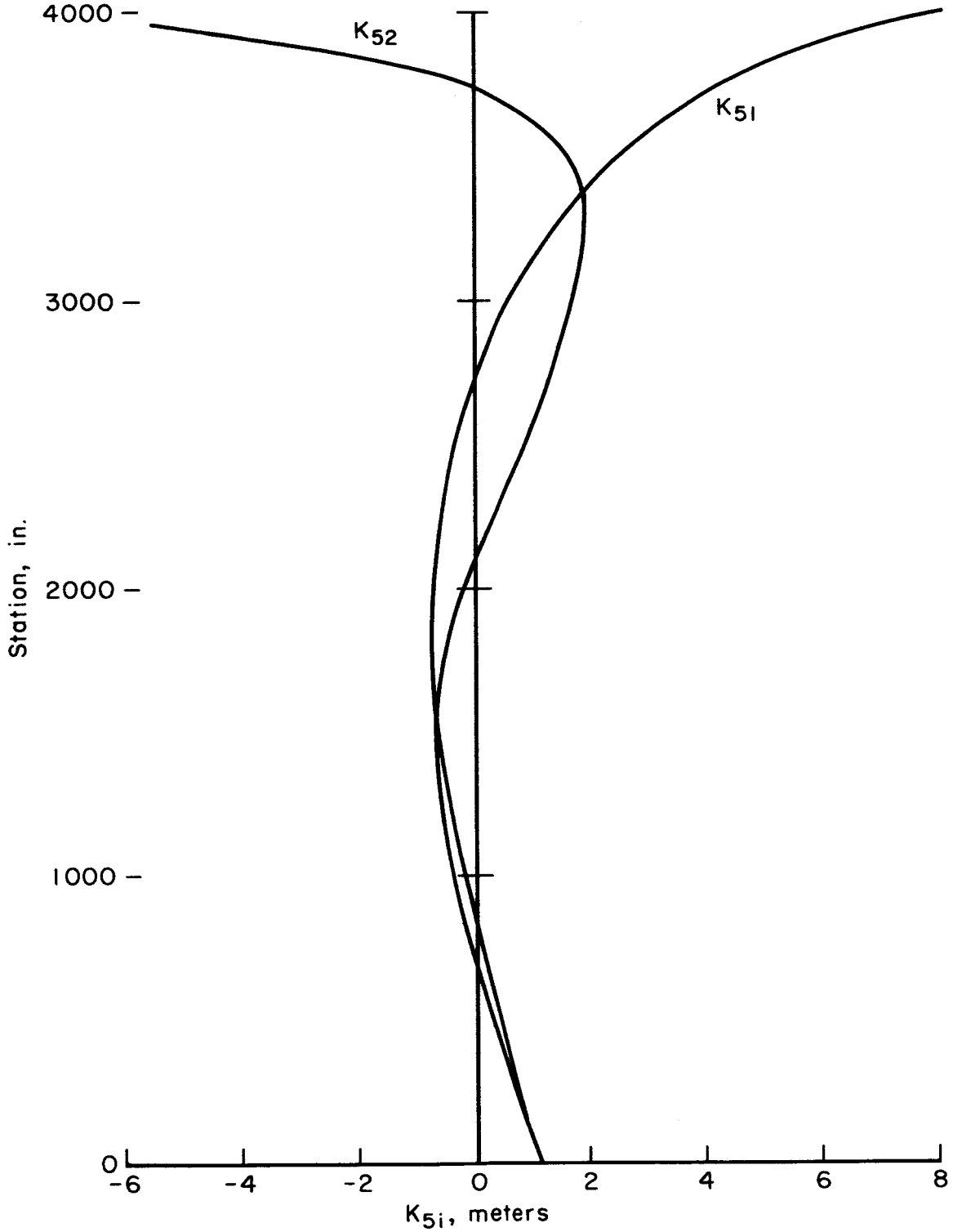

(b) Maximum q (t = 77 sec).

Figure 10.- Continued.

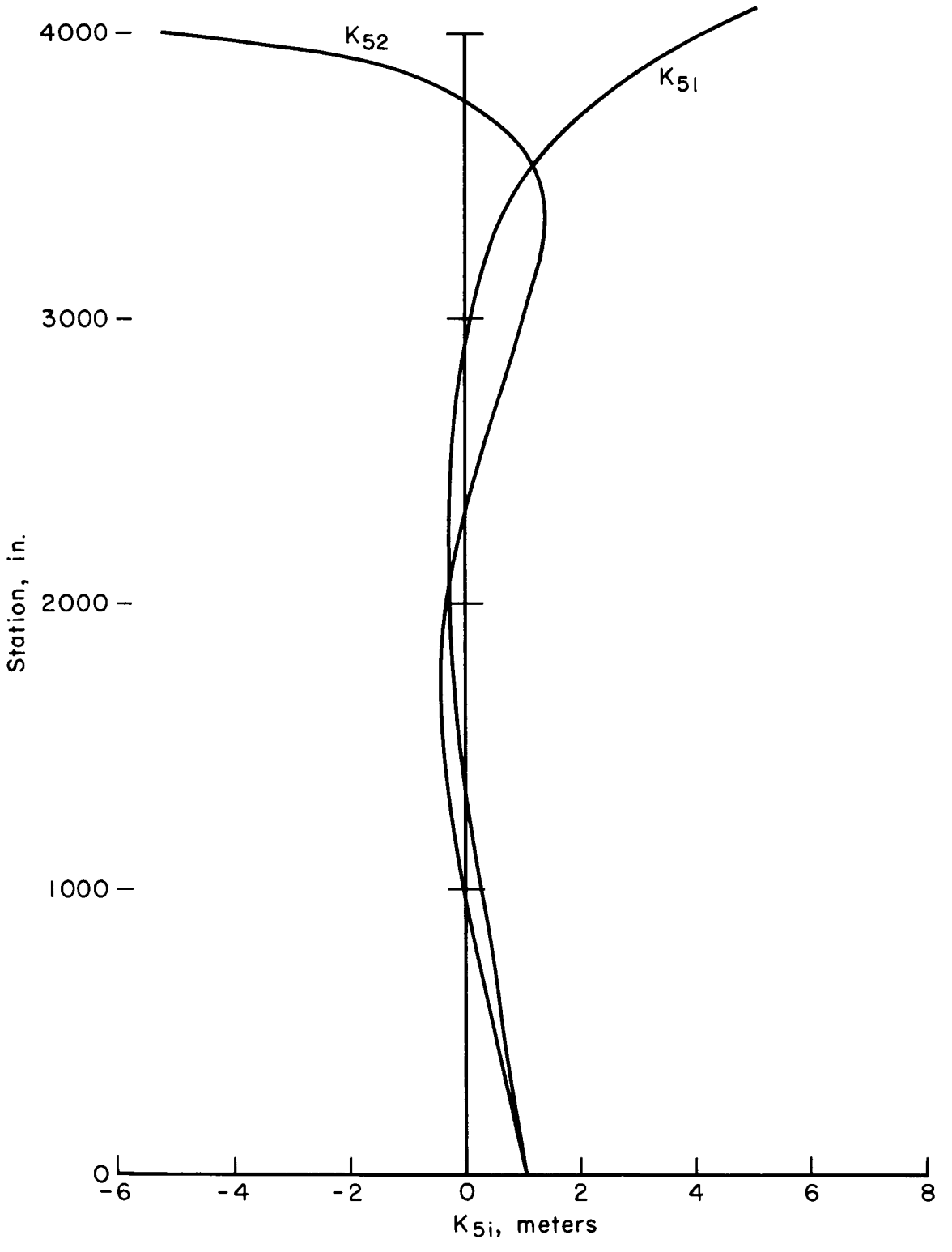

(c) Burnout (t = 150 sec).

Figure 10.- Concluded.

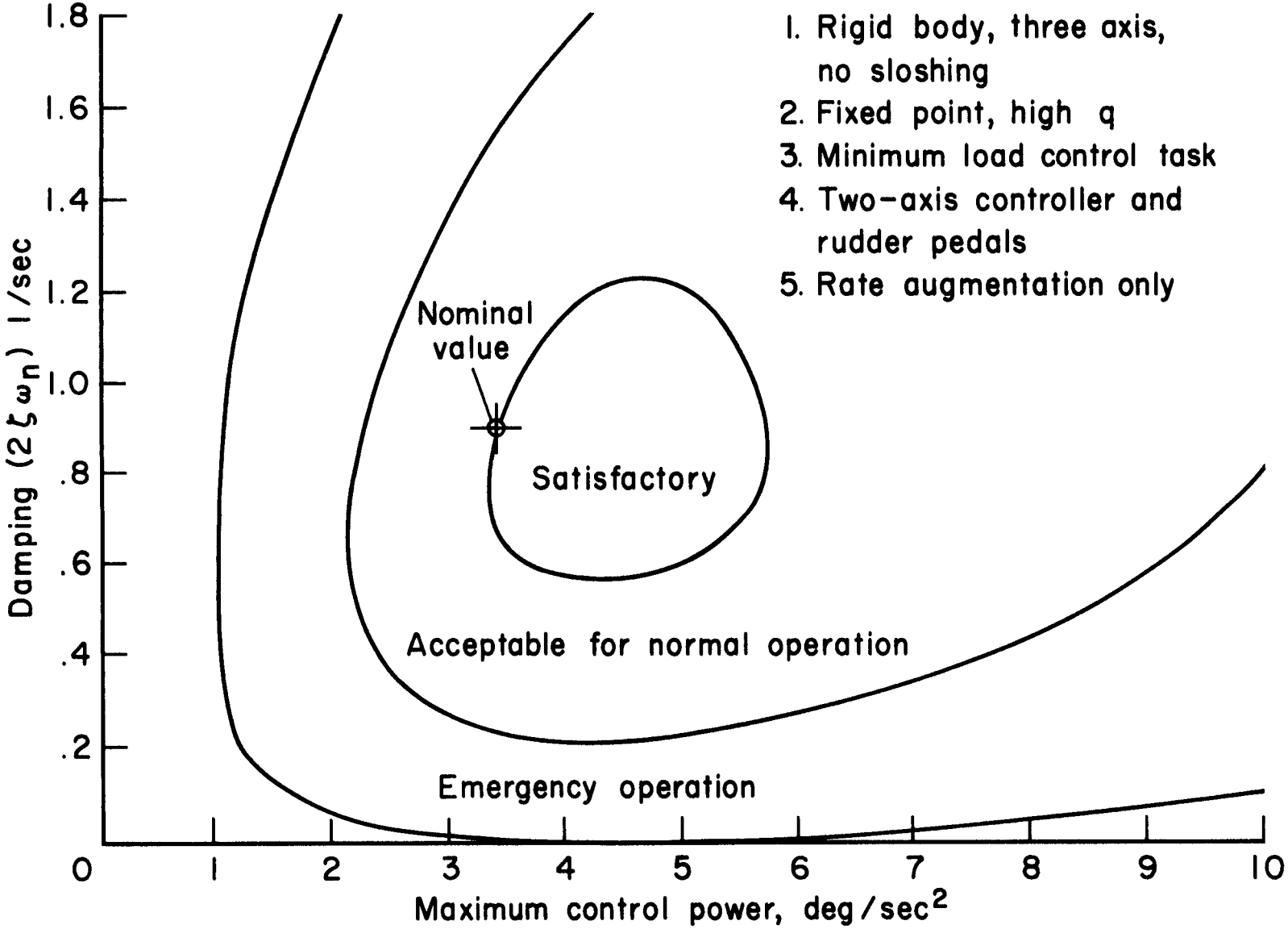

Figure 11.- Piloted boost control boundaries.

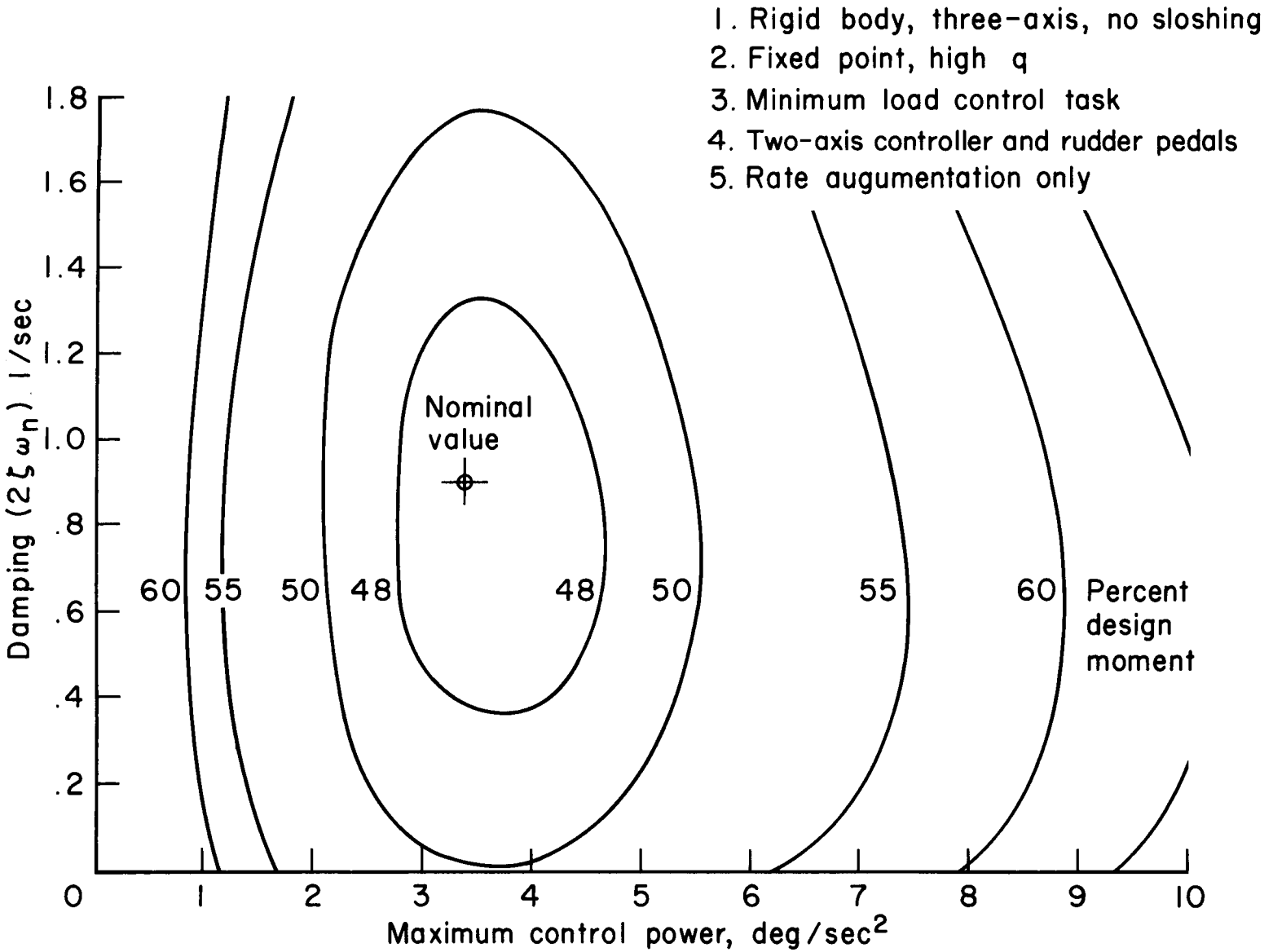

Figure 12.- Piloted boost performance.

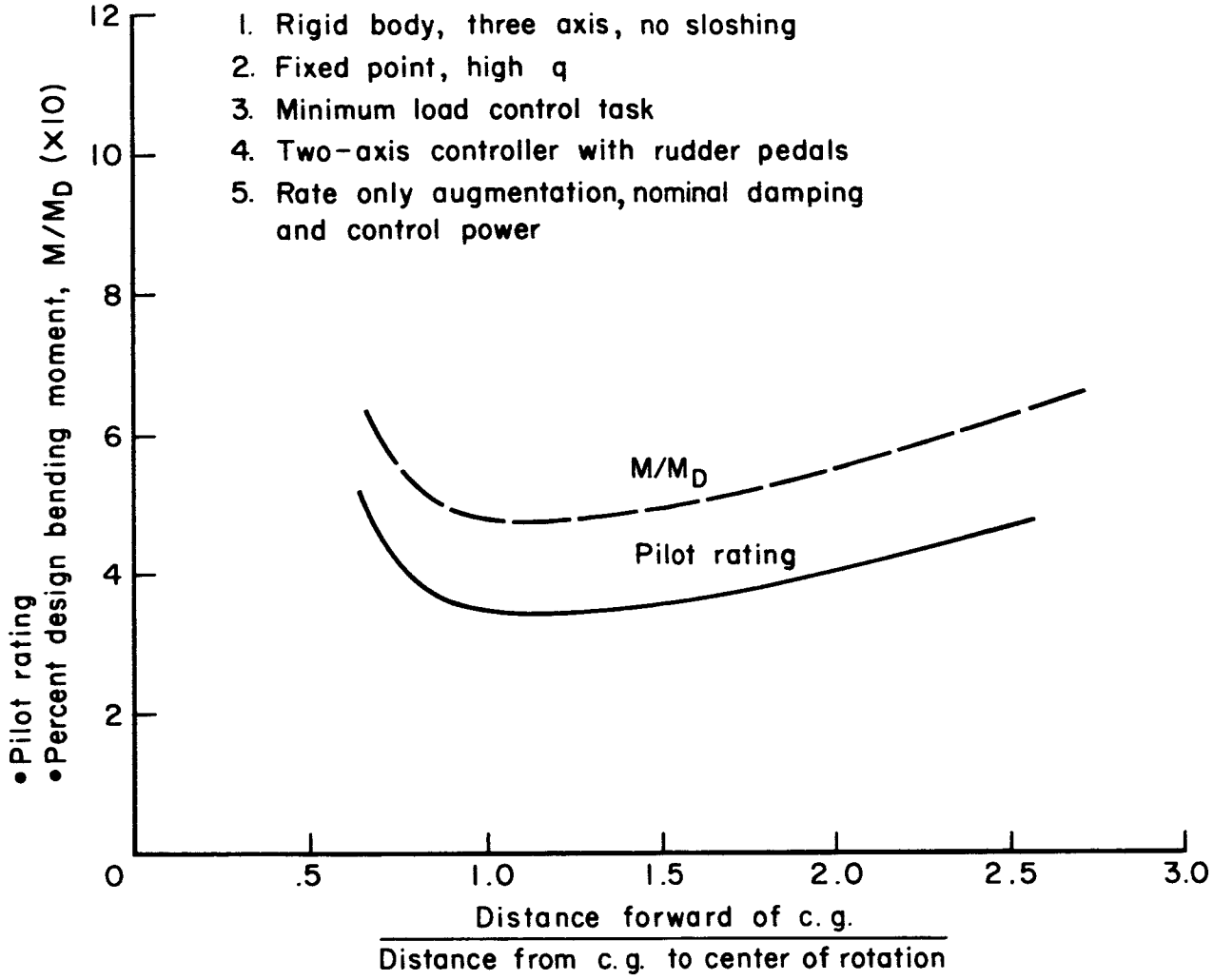

Figure 13.- Display accelerometer location.

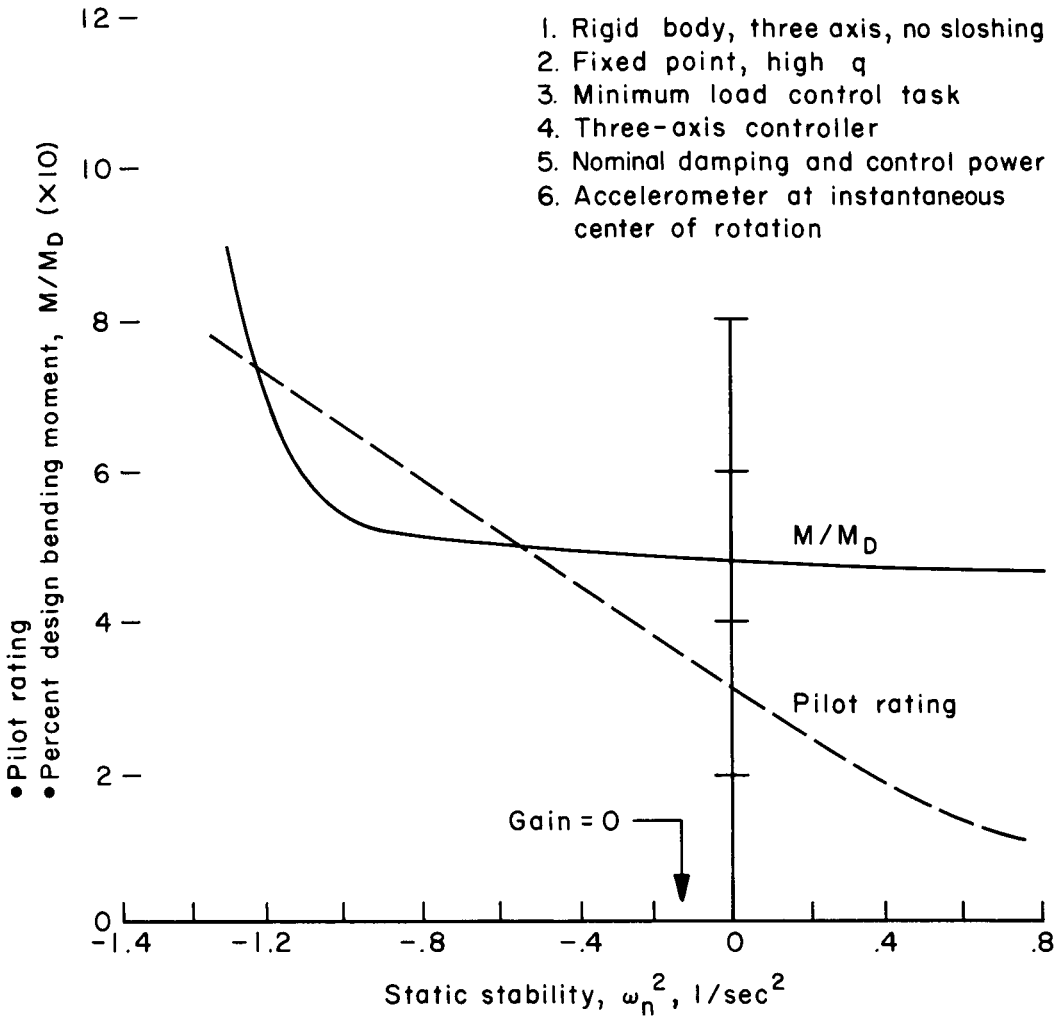

Figure 14.- Accelerometer augmentation.

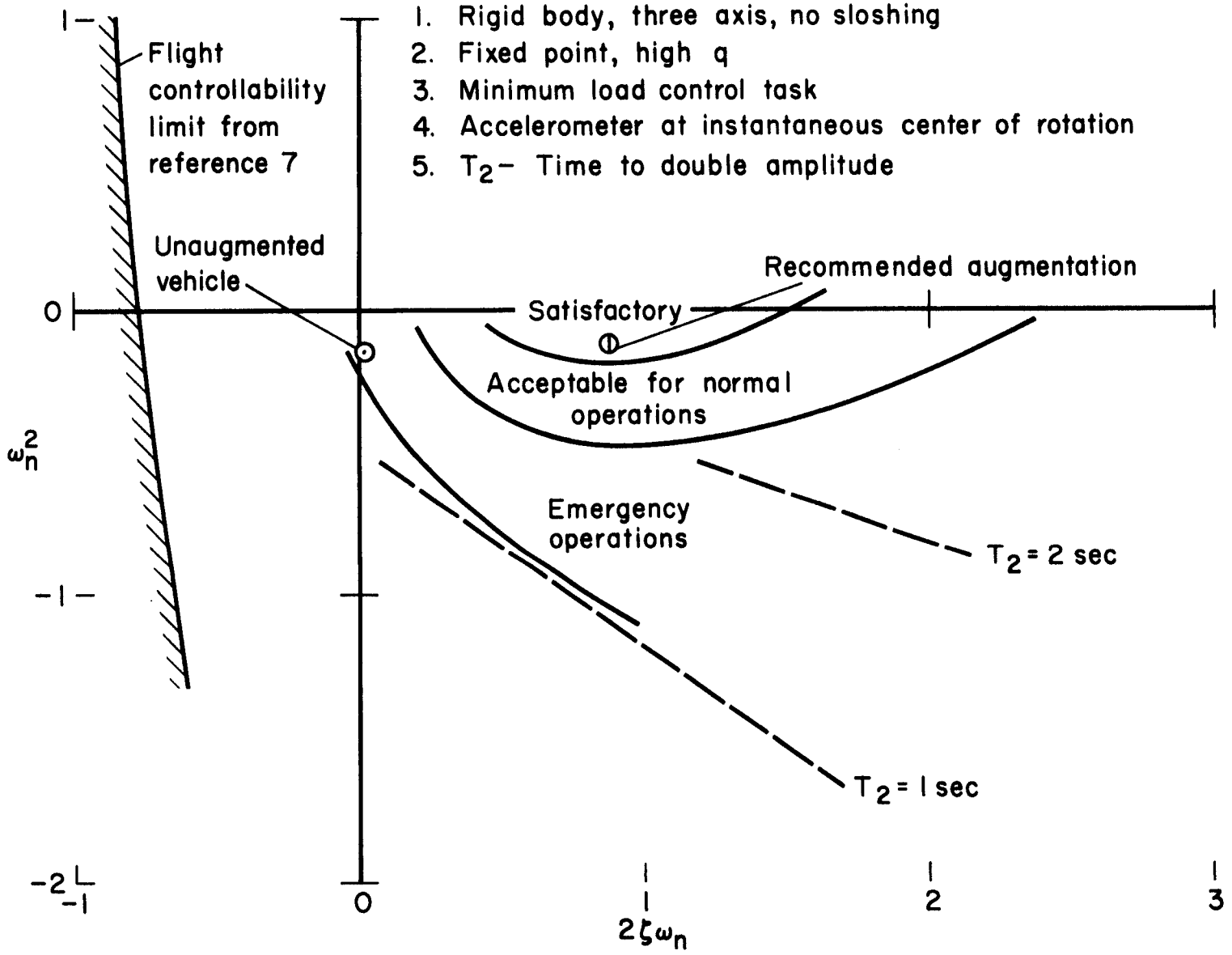

Figure 15.- Basic handling qualities.

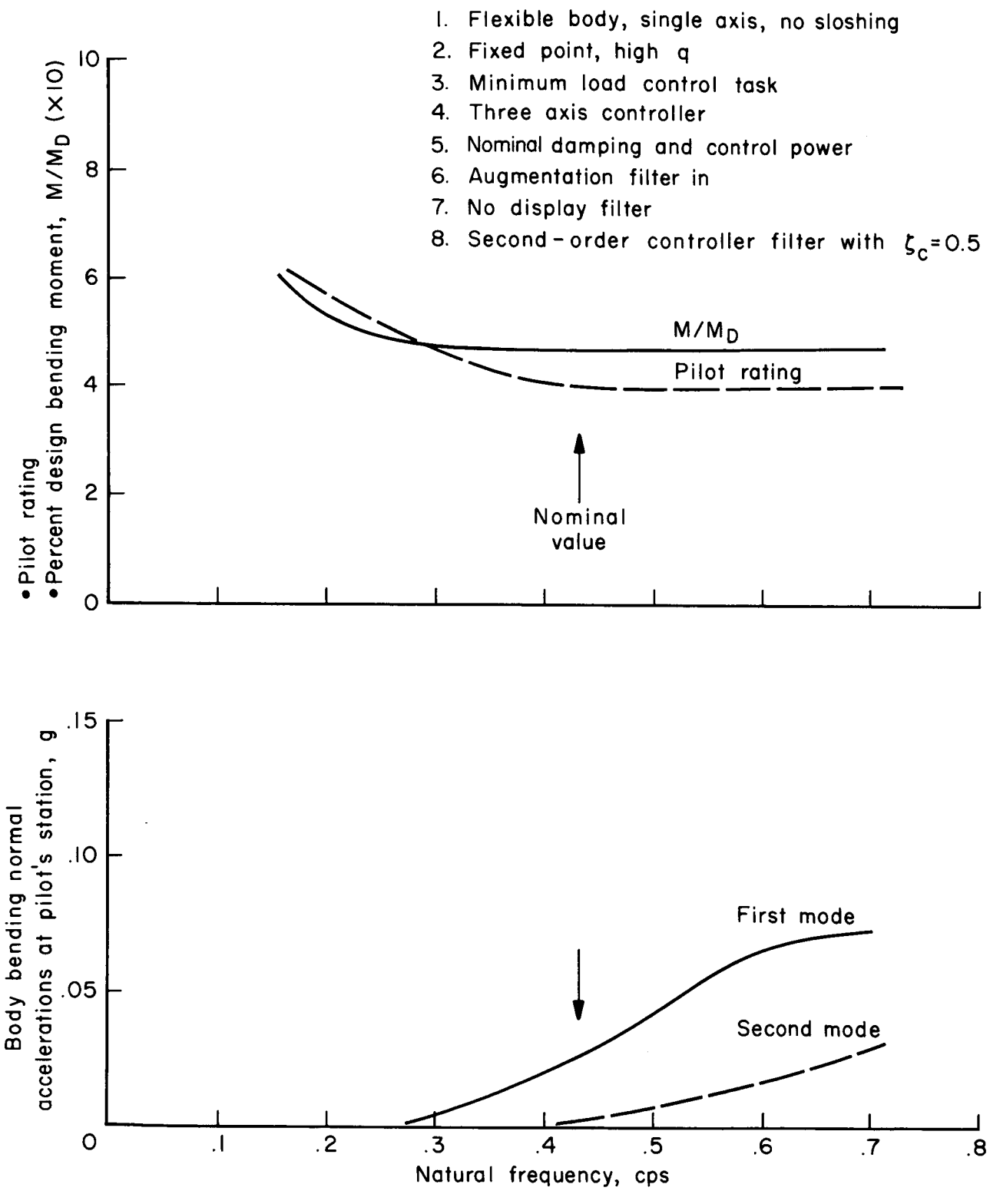

Figure 16.- Controller filter.

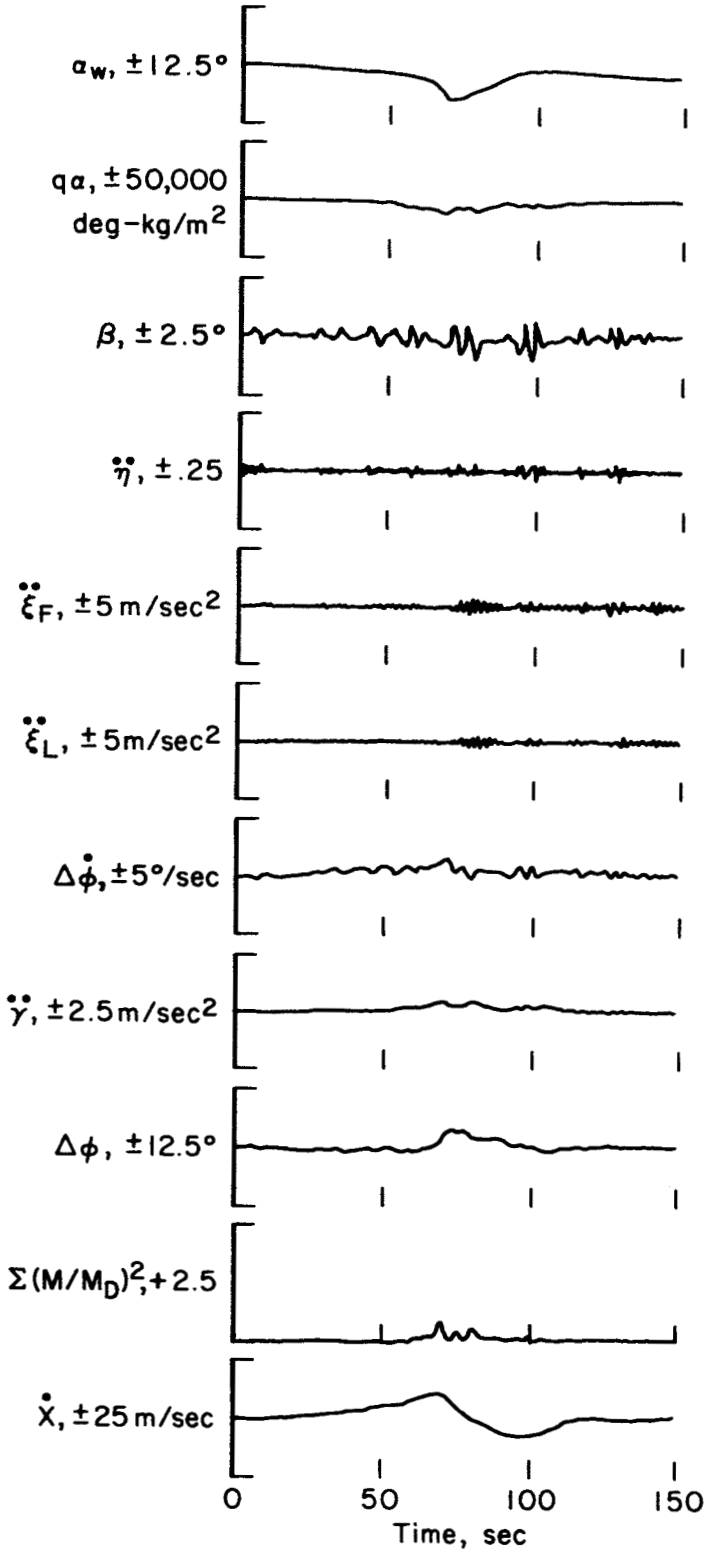

Figure 17.- Typical run (only pitch recorded).

1. Continuous time of flight simulation
2. Elastic body with sloshing
3. Design damping and control power
4. Nominal augmentation and controller filters

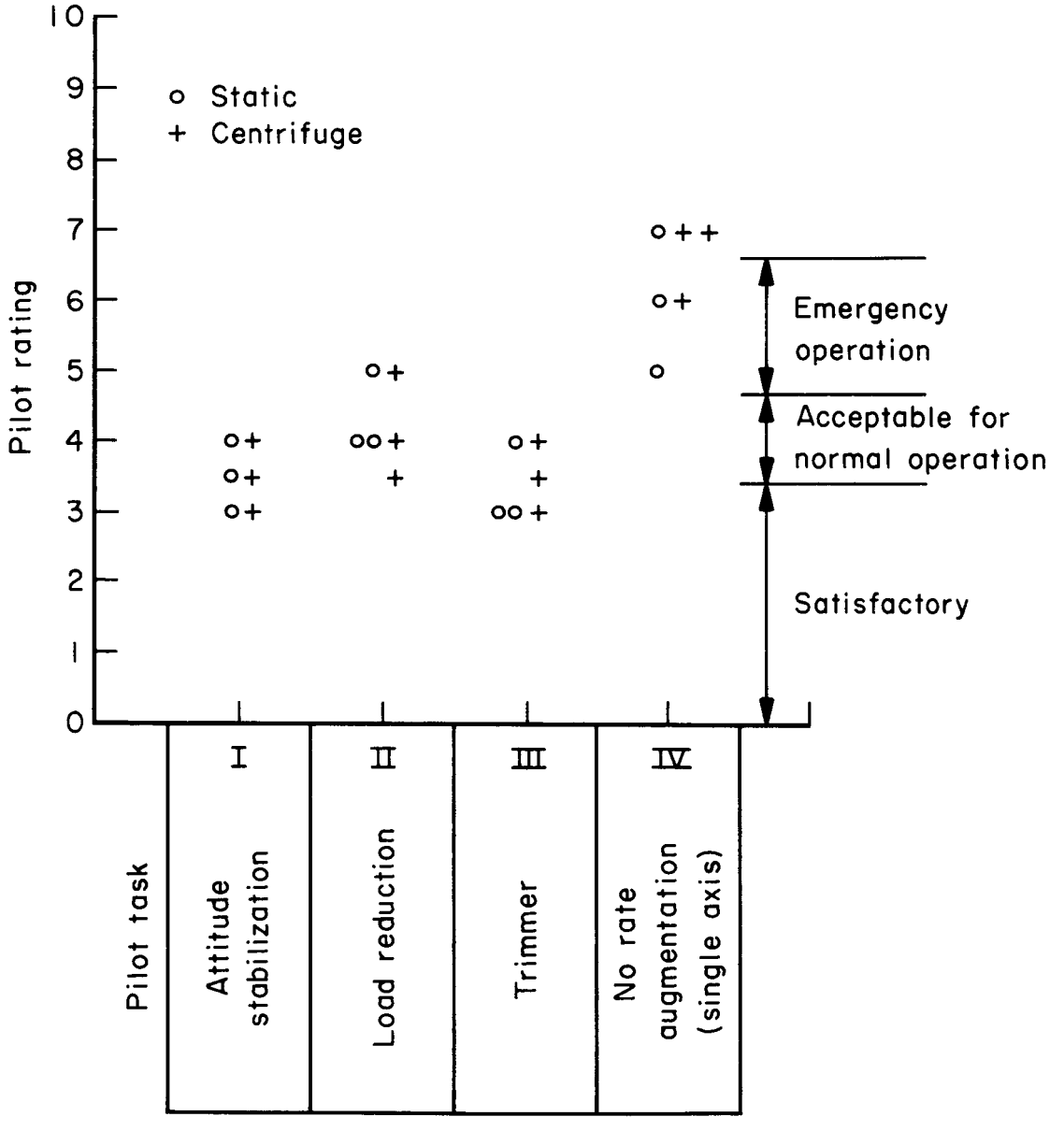

Figure 18.- Pilot rating.

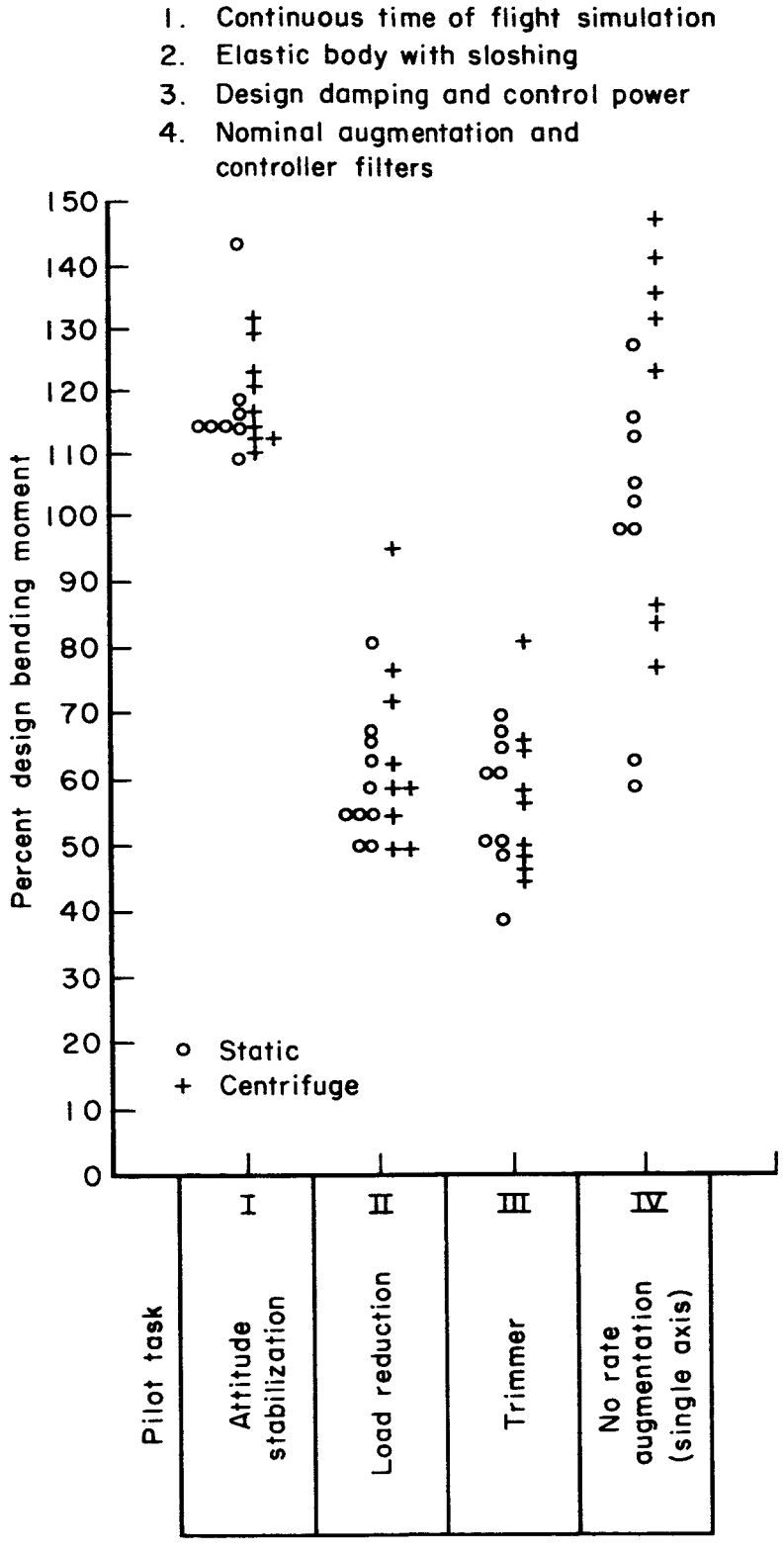

Figure 19.- Structural load.

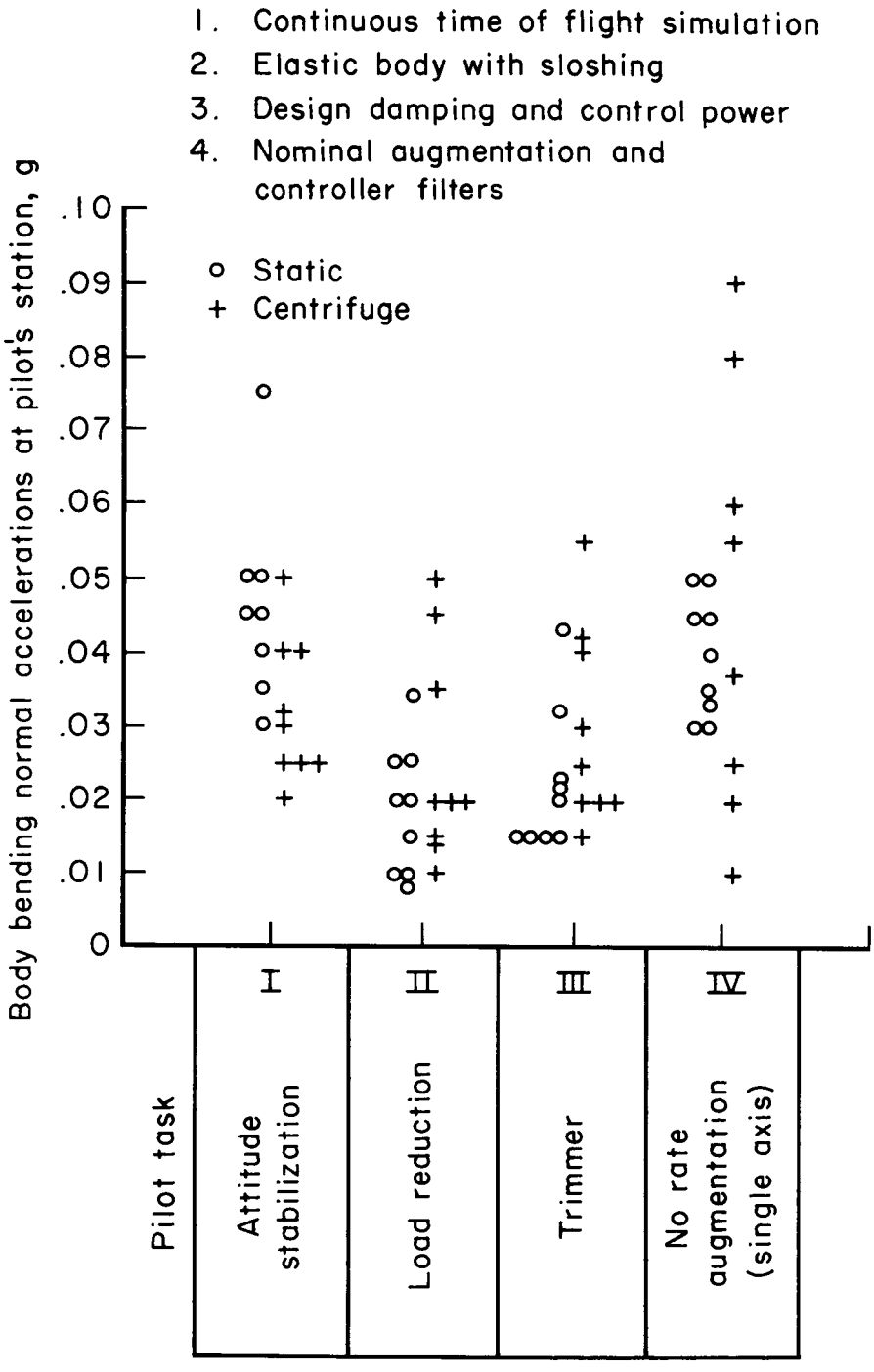

Figure 20.- Body elastic motions.

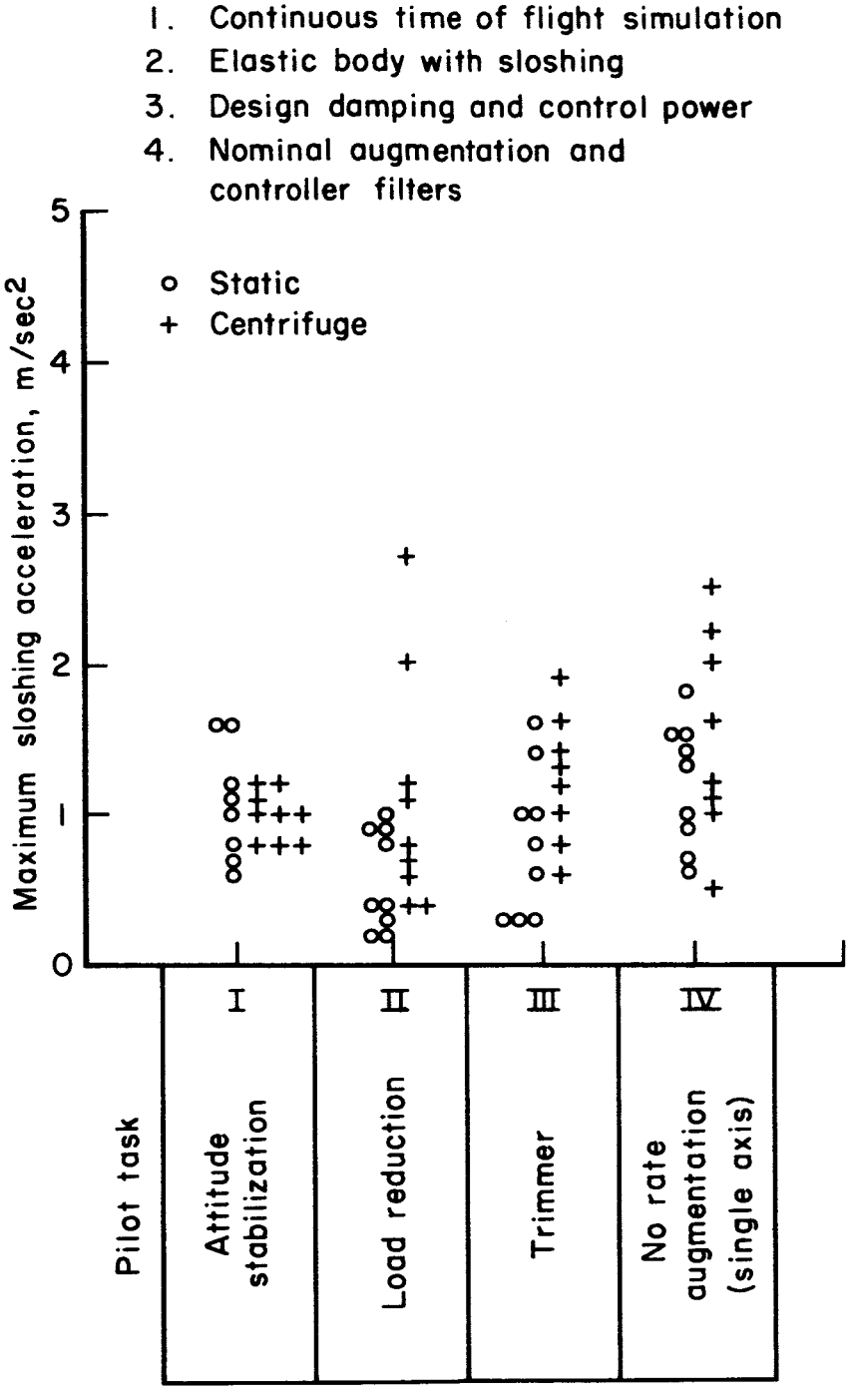

Figure 21.- Sloshing dynamics.

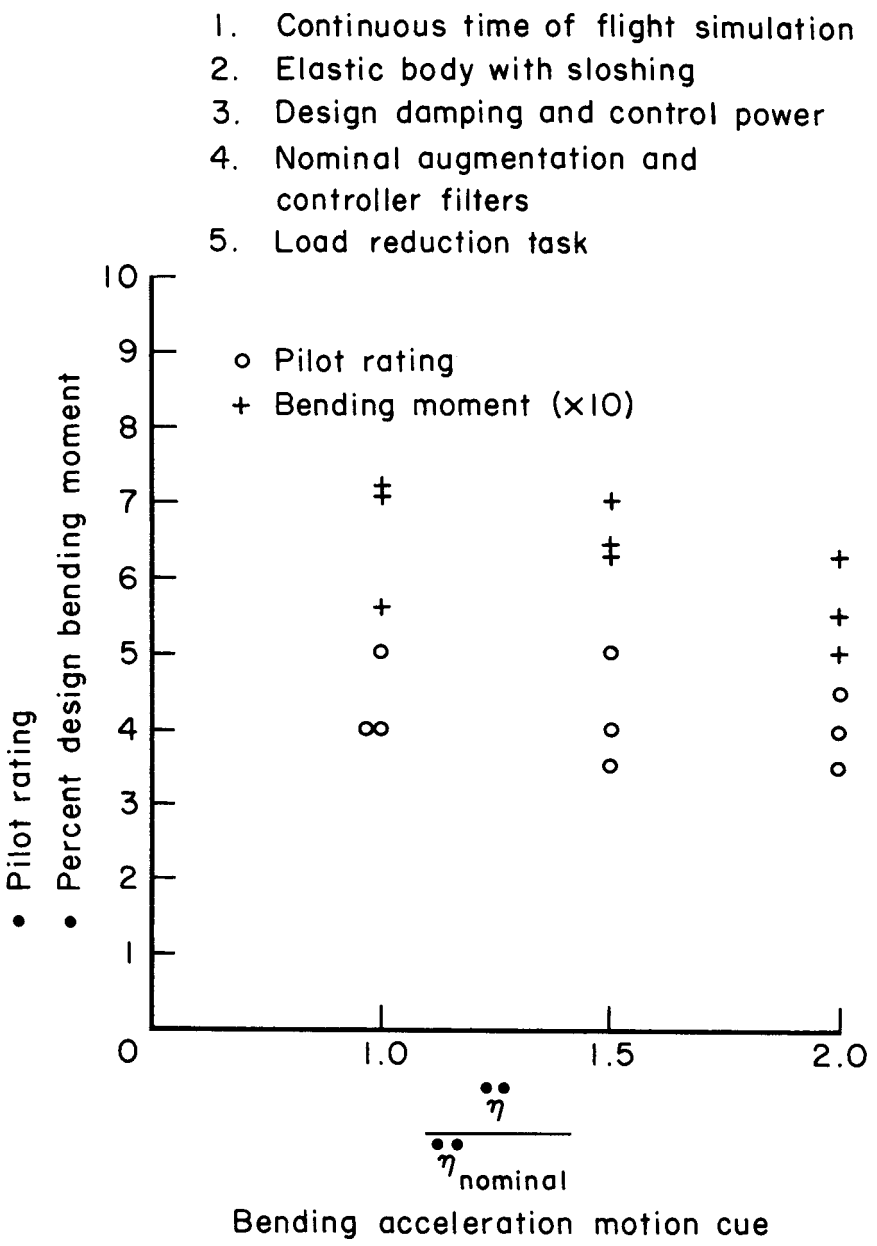

Figure 22.- Elastic motion cues.

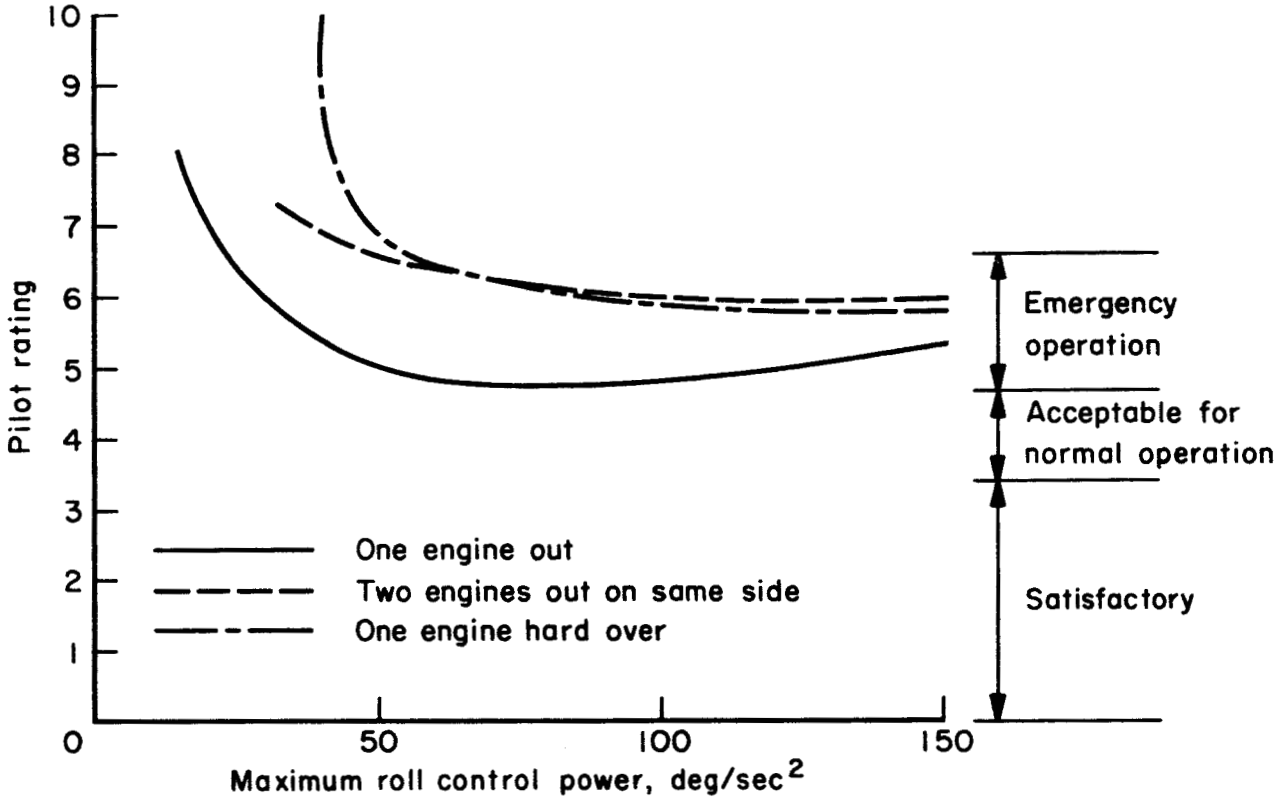

Figure 23.- Roll control power.

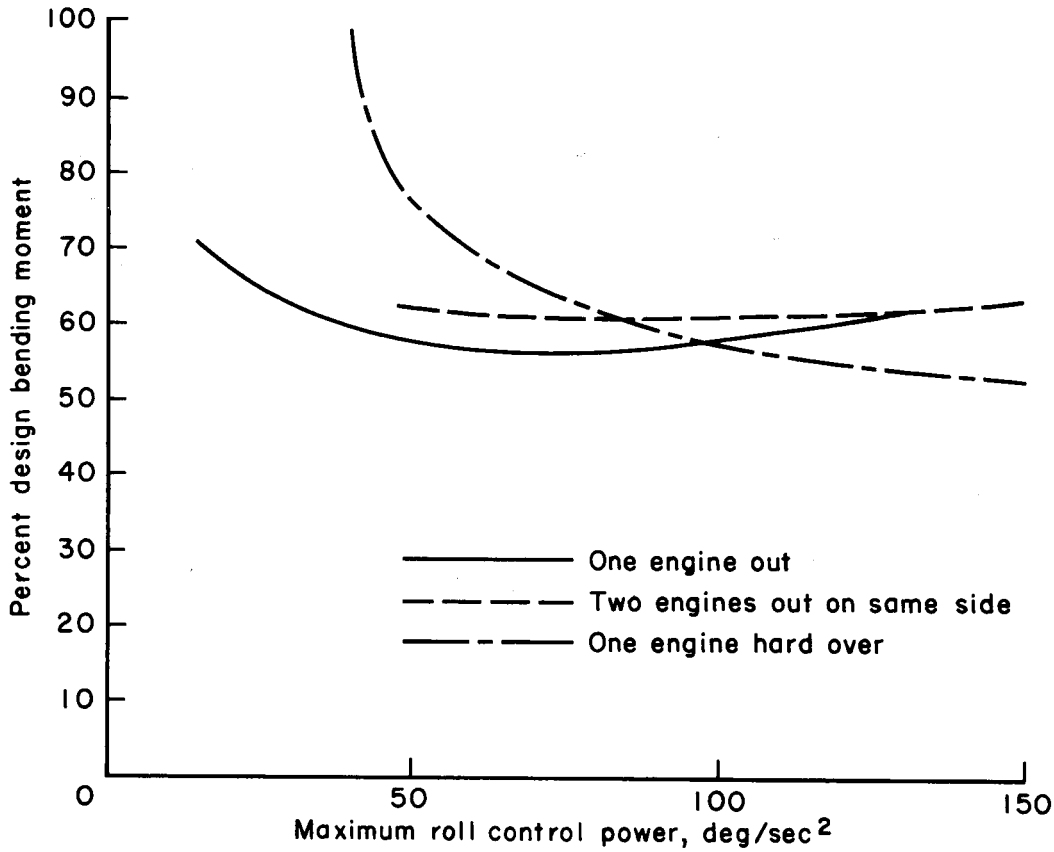

Figure 24.- Roll control power.

Failure mode	Time of failure		
	$0<t<60$	$60<t<105$	$105<t<150$
One engine out	0 0 0 0 0 0 0 0 0	0 0 0 0 X_1 0 0 0 0	0 0 0 0 0 0 0 0 0
Two engines out	0 0 0 0 X_1 0 0 X_1 0	0 X_1 X_2 0 0 X_2 0 0 X_2	0 0 0 0 0 0 0 0 0
One engine hard over	0 0 0 0 0 X_1 0 0 0	X_1 X_2 $X_{1,2}$ 0 X_2 $X_{1,2}$ X_1 $X_{1,2}$ $X_{1,2}$	0 0 0 0 0 0 0 0 0
Rate gyro out	X_1 0 X_1 0 X_1 0 0 X_1 X_1	0 X_2 $X_{1,2}$ 0 X_2 $X_{1,2}$ 0 X_2 $X_{1,2}$	0 0 0 0 0 0 0 0 0
$\Delta\phi = 0$	0 0 0 0 0 0 0 0 0	0 0 0 0 0 0 0 0 0	0 0 0 0 0 0 0 0 0
Trimmer mode rate out	X_1 X_1 X_1 X_1 $X_{1,3}$ $X_{1,3}$ 0 X_1 0	0 $X_{1,2}$ $X_{1,2}$ 0 $X_{1,2}$ X_2 0 $X_{1,2}$ $X_{1,2}$	0 0 0 0 0 0 0 0 0

A. Worst wind direction (fig 2) used in all cases

B. Performance criteria exceeded:

X_1 - $M/M_D > 100$ percent

X_2 - Pilot rating > 6.5

X_3 - Pitch or yaw rate > 4°/sec
(Emergency abort system actuated)

Figure 25.- Emergency mode performance.

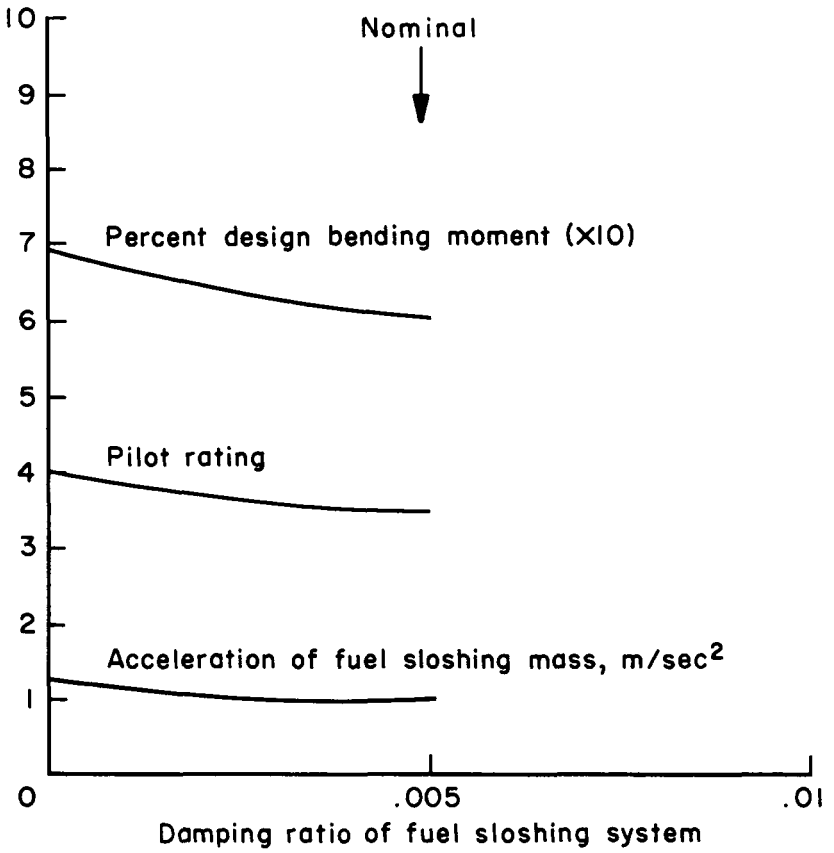

Figure 26.- Fuel sloshing damping ratio.

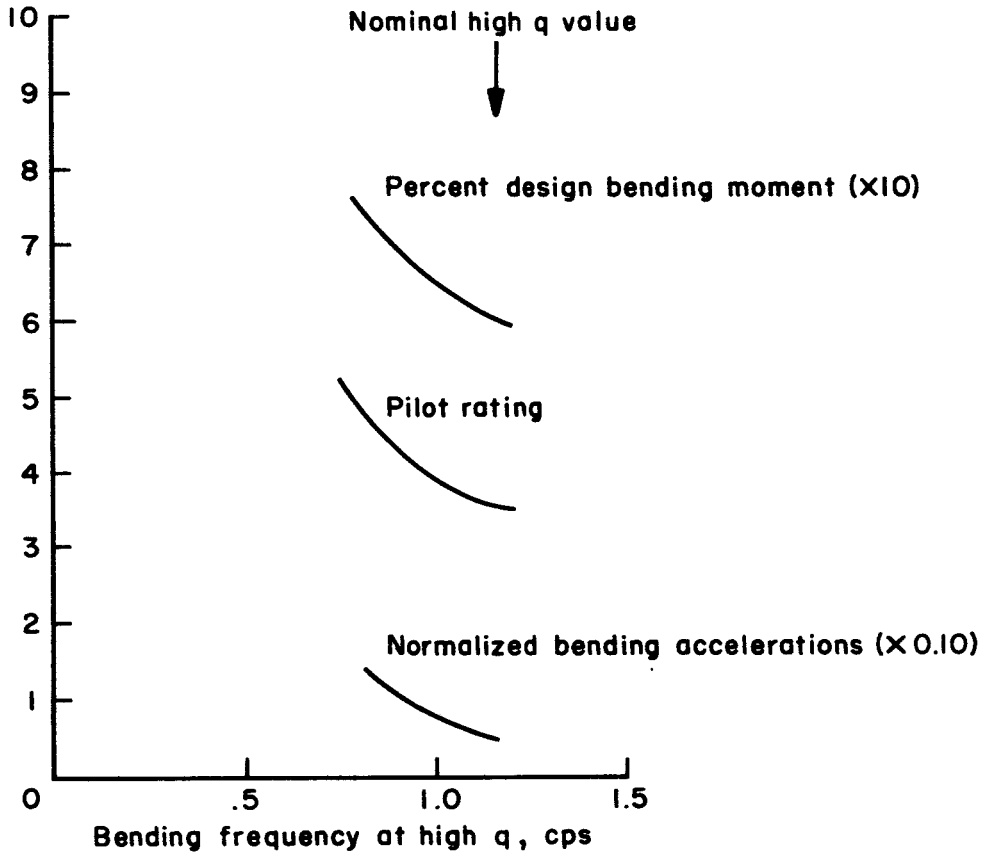

Figure 27.- First elastic mode frequency.

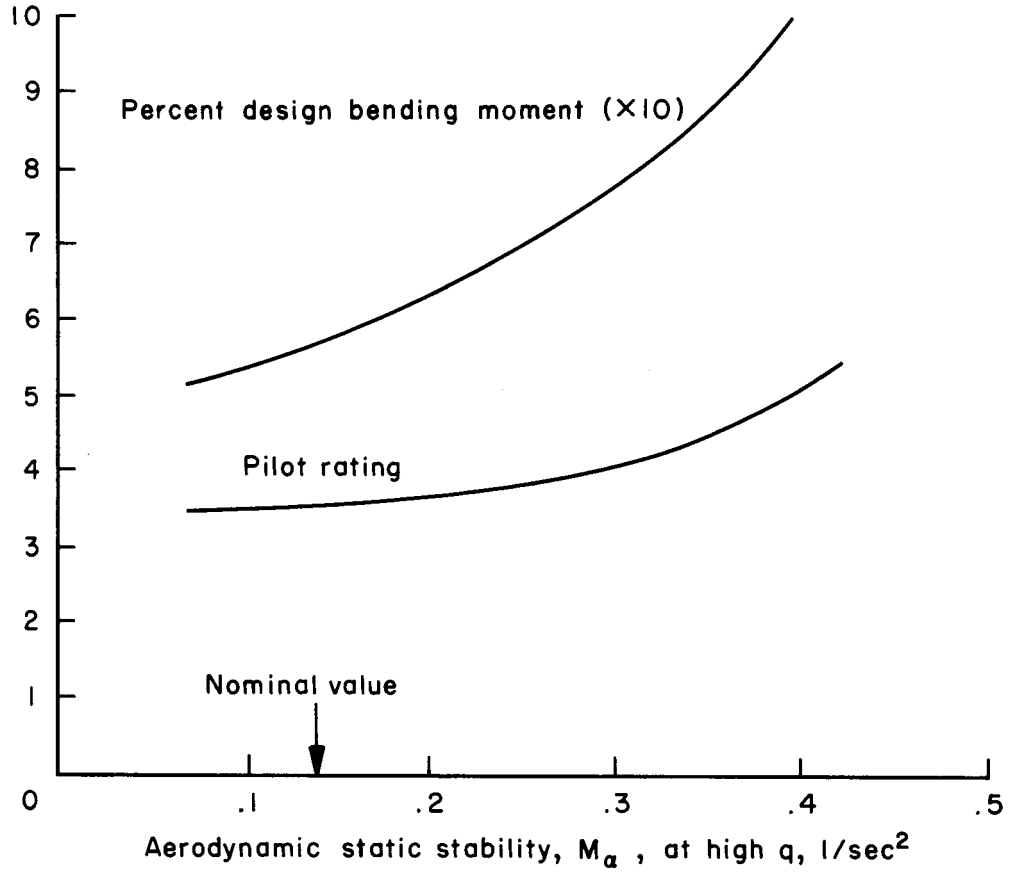

Figure 28.- Aerodynamic static stability.

NASA-Langley, 1965 A-1010